Article

Neuron

Connexin 43-Mediated Astroglial Metabolic Networks Contribute to the Regulation of the Sleep-Wake Cycle

Highlights

- Cx43-mediated gap junctions are functional in the lateral hypothalamus
- Astroglial Cx43 permit lactate shuttling from astrocytic networks to orexin neurons
- Knockout of astroglial Cx43 silences orexin neurons, causing wakefulness instability
- Lactate delivery to the lateral hypothalamic area rescues normal wakefulness

Authors

Jerome Clasadonte, Eliana Scemes, Zhongya Wang, Detlev Boison, Philip G. Haydon

Correspondence

jerome.clasadonte@inserm.fr (J.C.), philip.haydon@tufts.edu (P.G.H.)

In Brief

Astrocytes supply energy metabolites to neurons, but how this influences behavior is unclear. Clasadonte et al. demonstrate that delivery of lactate from astrocytes to neurons is required for normal orexinergic neuronal activity and hence daily cycles of wakefulness.

Clasadonte et al., 2017, Neuron *95*, 1–16
September 13, 2017
http://dx.doi.org/10.1016/j.neuron.2017.08.022

CellPress

Please cite this article in press as: Clasadonte et al., Connexin 43-Mediated Astroglial Metabolic Networks Contribute to the Regulation of the Sleep-Wake Cycle, Neuron (2017), http://dx.doi.org/10.1016/j.neuron.2017.08.022

Neuron
Article

Connexin 43-Mediated Astroglial Metabolic Networks Contribute to the Regulation of the Sleep-Wake Cycle

Jerome Clasadonte,[1,2,3,*] Eliana Scemes,[4] Zhongya Wang,[5] Detlev Boison,[5] and Philip G. Haydon[1,6,*]
[1]Department of Neuroscience, Tufts University School of Medicine, Boston, MA, USA
[2]Inserm, Laboratory of Development and Plasticity of the Neuroendocrine Brain, Jean-Pierre Aubert Research Center, U1172, Lille, France
[3]University of Lille, FHU 1000 days for Health, School of Medicine, Lille, France
[4]Dominick P. Purpura Department of Neuroscience, Albert Einstein College of Medicine, Bronx, NY, USA
[5]Robert Stone Dow Neurobiology Laboratories, Legacy Research Institute, Portland, OR, USA
[6]Lead Contact
*Correspondence: jerome.clasadonte@inserm.fr (J.C.), philip.haydon@tufts.edu (P.G.H.)
http://dx.doi.org/10.1016/j.neuron.2017.08.022

SUMMARY

Astrocytes produce and supply metabolic substrates to neurons through gap junction-mediated astroglial networks. However, the role of astroglial metabolic networks in behavior is unclear. Here, we demonstrate that perturbation of astroglial networks impairs the sleep-wake cycle. Using a conditional Cre-Lox system in mice, we show that knockout of the gap junction subunit connexin 43 in astrocytes throughout the brain causes excessive sleepiness and fragmented wakefulness during the nocturnal active phase. This astrocyte-specific genetic manipulation silenced the wake-promoting orexin neurons located in the lateral hypothalamic area (LHA) by impairing glucose and lactate trafficking through astrocytic networks. This global wakefulness instability was mimicked with viral delivery of Cre recombinase to astrocytes in the LHA and rescued by in vivo injections of lactate. Our findings propose a novel regulatory mechanism critical for maintaining normal daily cycle of wakefulness and involving astrocyte-neuron metabolic interactions.

INTRODUCTION

Sleep plays a vital role in health and well-being and is critical for immune function, metabolism, and memory and learning (Brown et al., 2012). While major progress has been made in understanding functions of sleep, mechanisms underlying its regulation are unclear (Brown et al., 2012). It was only recently that astrocytes were implicated in sleep mechanisms and functions through their regulation of gliotransmission (Halassa et al., 2009; Paukert et al., 2014; Araque et al., 2014).

Astrocytes form an extensive network of cells interconnected through gap junction channels formed by connexin (Cx) proteins (Goodenough et al., 1996). Gap junctions allow the passage of small molecules including ions, second messengers, and energy metabolites such as glucose and lactate (see Giaume et al., 2010). Cx43, the major constituent of gap junctions in astrocytes, is highly expressed throughout the brain (Nagy and Rash, 2000). The Cre-Lox conditional knockout (cKO) approach is often used to investigate the physiological functions of astroglial Cx43 and astrocytic networks in the CNS (Giaume et al., 2010; Giaume and Theis, 2010; Pannasch and Rouach, 2013; Oliveira et al., 2015). The use of Cx43 cKO^{GFAP} mice with Cre transgenic lines under the promoter of a human glial fibrillary acidic protein (Cx43$^{f/f}$:hGFAP-Cre; Theis et al., 2003; Wiencken-Barger et al., 2007) has demonstrated the contribution of Cx43 hemichannels and Cx43-mediated gap junctions to neuron-glia interactions (Giaume et al., 2010; Giaume and Theis, 2010; Pannasch and Rouach, 2013, Oliveira et al., 2015) and to metabolic coupling between neurons and astrocytes (Rouach et al., 2008). This latter process is based on the "astrocyte to neuron lactate shuttle" (ANLS) hypothesis (Pellerin and Magistretti, 1994), in which glucose is taken up by astrocyte endfeet and enters the glycolytic pathway to be converted into lactate, which is then transported through the gap junction-mediated astrocytic network to fuel neuronal energy demands (Rouach et al., 2008). Although recent studies suggest a role for astroglial Cx43 in neuroglial interactions, their contribution to physiological brain functions such as sleep remains largely unknown.

We performed cortical electroencephalographic (EEG) and electromyographic (EMG) recordings in Cx43 cKO^{GFAP} mice (Wiencken-Barger et al., 2007; Han et al., 2014) to determine the role of astroglial Cx43 on sleep-wake regulation. Cx43 cKO^{GFAP} mice exhibited excessive sleepiness and fragmented wakefulness during the nocturnal active phase. We show that orexin (hypocretin)-producing neurons (orexin neurons) in the lateral hypothalamic area (LHA), crucial regulators of wakefulness (Sakurai, 2007), have reduced activity in Cx43 cKO^{GFAP} mice. This reduced activity was due to an attenuated diffusion of energy metabolites, glucose and lactate, through gap junction-mediated astrocytic networks in the LHA. Viral transduction of astrocytes in the LHA of Cx43$^{f/f}$ littermate controls mimicked the sleep phenotype of cKO animals by promoting sleepiness and fragmented wakefulness during the nocturnal active phase.

This phenotype was rescued by chronic delivery of lactate into the LHA. We demonstrate that an astrocytic source of lactate trafficking through the Cx43-mediated astrocytic gap junctions in the LHA is crucial for normal activity of orexin neurons and, consequently, for wakefulness.

RESULTS

Deletion of Cx43 in Astrocytes Decreases Wakefulness during the Active Phase

To investigate the role of astroglial Cx43 in sleep-wake regulation, we combined cortical EEG and EMG recordings with the Cx43$^{f/f}$:hGFAP-Cre mouse (Wiencken-Barger et al., 2007; Han et al., 2014), which allowed us to knock out the *Gja1* gene encoding Cx43 selectively in astrocytes. To generate Cx43$^{f/f}$:hGFAP-Cre (Cx43 cKO^{GFAP}) mice, homozygous Cx43$^{f/f}$ mice (Liao et al., 2001) were crossed to hGFAP-Cre mice (Casper and McCarthy, 2006), in which the Cre recombinase is under the control of the human glial GFAP promoter (Figure 1A). PCR was used to identify the correct genotypes (Figure 1B), and the efficiency and specificity of *Gja1* gene deletion in astrocytes in the Cx43 cKO^{GFAP} mice were characterized previously (Wiencken-Barger et al., 2007; Han et al., 2014). Western blots demonstrated that Cx43 expression was substantially reduced in brains of Cx43 cKO^{GFAP} mice compared to Cx43$^{f/f}$ littermates and WT mice with the same C57BL/6J inbred background (Figure 1C).

EEG/EMG recordings for 24 hr indicated that Cx43$^{f/f}$ and Cx43 cKO^{GFAP} mice displayed a normal circadian sleep-wake rhythm (Figure 1D). However, Cx43 cKO^{GFAP} mice showed changes in vigilance state distribution during the dark phase (Figure 1D). The time spent awake in Cx43 cKO^{GFAP} mice was reduced by 23.76% during the 12 hr dark phase, when mice are typically active (Figure 1E). This reduction was concomitant with a significant increase in time spent in non-rapid eye movement (NREM) sleep (56.73%), rapid eye movement (REM) sleep (141.88%), and total sleep time (TST including REM + NREM sleep: 59.79%; Figure 1E). These results indicate that deficiency in astroglial Cx43 induces sleepiness during the nocturnal active phase.

Cx43 Deletion in Astrocytes Causes Wakefulness Instability during the Active Phase

Cx43 cKO^{GFAP} were unable to sustain a period of consolidated wakefulness especially during the first 6 hr of the dark phase (zeitgeber time [ZT] 12-ZT18; Figure 1F). Intrusions of short periods of NREM sleep were frequently found within periods of wakefulness at the beginning of the dark phase (Figure 1F). In addition, Cx43 cKO^{GFAP} mice had more episodes of wakefulness during both light and dark phases (Figure 1G), although of shorter duration (Figure 1H). Cx43 cKO^{GFAP} mice also had more episodes of NREM and REM sleep, but only during the dark phase (Figure 1G) and with a duration that remained unchanged (Figure 1H). This increase in episode numbers of wakefulness, NREM, and REM sleep in Cx43 cKO^{GFAP} mice during dark phase was associated with an increase in the number of transitions between all vigilance states (Figure 1I), demonstrating that these mice had difficulty in sustaining long episodes of wakefulness.

Cx43 Deletion in Astrocytes Decreases Spontaneous Firing Frequency and Excitability in Orexin Neurons

Since excessive sleepiness and instability of wakefulness during the active phase is reminiscent of narcolepsy due to the loss of wake-promoting orexin neurons in the LHA (Sakurai, 2007), we investigated whether Cx43 cKO^{GFAP} mice caused changes in orexin neurons. Immunohistochemistry against orexin-A (ORX-A), the main isoform of orexin involved in the regulation of wakefulness (Sakurai, 2007), showed that the number of ORX-A-positive cells was similar in both genotypes (Figure S1).

Since electrical activity of orexin neurons changes across the sleep-wake cycle (Mileykovskiy et al., 2005; Lee et al., 2005; Adamantidis et al., 2007; Hassani et al., 2009; Tsunematsu et al., 2011), we used whole-cell current-clamp recordings in acute brain slices to ask whether astroglial Cx43 modulates the activity of orexin neurons. Orexin neurons were identified based on their electrophysiological characteristics (Eggermann et al., 2003; Parsons and Hirasawa, 2010), such as tonic spontaneous firing (Figure 2A1), H-current (Figure S2A), monophasic after hyperpolarizing potential (AHP; Figure S2A), and low-threshold spike (Figure S2A). Recorded cells were filled with biocytin for post hoc histological verification of ORX-A-expressing neurons (Figures 2A2 and 2B2). With an artificial cerebrospinal fluid (ACSF) containing a physiological concentration of glucose (2.5 mM; Parsons and Hirasawa, 2010; Sada et al., 2015), orexin neurons from Cx43 cKO^{GFAP} mice displayed reduced spontaneous firing compared with Cx43$^{f/f}$ mice (Figures 2A1, 2B1, and 2C). This reduced basal firing persisted in loose patch-clamp configuration (Figures 2D–2F), indicating that it was not a consequence of dilution of the intracellular compartment by whole-cell dialysis.

In Cx43 cKO^{GFAP} mice, orexin neurons fired fewer action potentials (APs) in response to depolarizing injected currents compared to Cx43$^{f/f}$ mice (Figures 2G, 2H, S2A, and S2B). The rate of increase in firing frequency during current ramps from 0 to +50 pA was decreased by 36% in orexin neurons from Cx43 cKO^{GFAP} mice (Cx43$^{f/f}$, 0.30 ± 0.01 Hz/pA, n = 15 cells, 9 mice; Cx43 cKO^{GFAP}, 0.19 ± 0.01 Hz/pA, n = 11 cells, 7 mice; Student's t test, $p < 0.001$; Figures 2G and 2H), while the slope of the AP output in response to current injection was decreased by 23% (Cx43$^{f/f}$, 0.34 ± 0.02 AP/pA, n = 14 cells, 9 mice; Cx43 cKO^{GFAP}, 0.26 ± 0.02 AP/pA, n = 12 cells, 6 mice; Student's t test, $p < 0.05$; Figure S2B). A more hyperpolarized resting membrane potential (RMP; Figure S2C) as well as a lower membrane input resistance (R_{in}; Figure S2D) were also observed in orexin neurons from the cKO animals. The slope of the current-voltage relationship from cKO animals was decreased compared with littermate controls (Figures S2A and S2E), resulting in the convergence of the two curves at −88 mV (Figure S2E), which is close to the potassium equilibrium potential in our conditions, suggesting that this effect was mediated by a potassium conductance.

Orexin Neurons Use Lactate as Energy Substrate

It has been previously suggested that orexin neurons rely on lactate as their main energy source (Parsons and Hirasawa, 2010). Since Cx43 gap junctions are critical for the trafficking of glucose and its metabolite, lactate, through the astrocytic networks during neuronal activity (Rouach et al., 2008), we

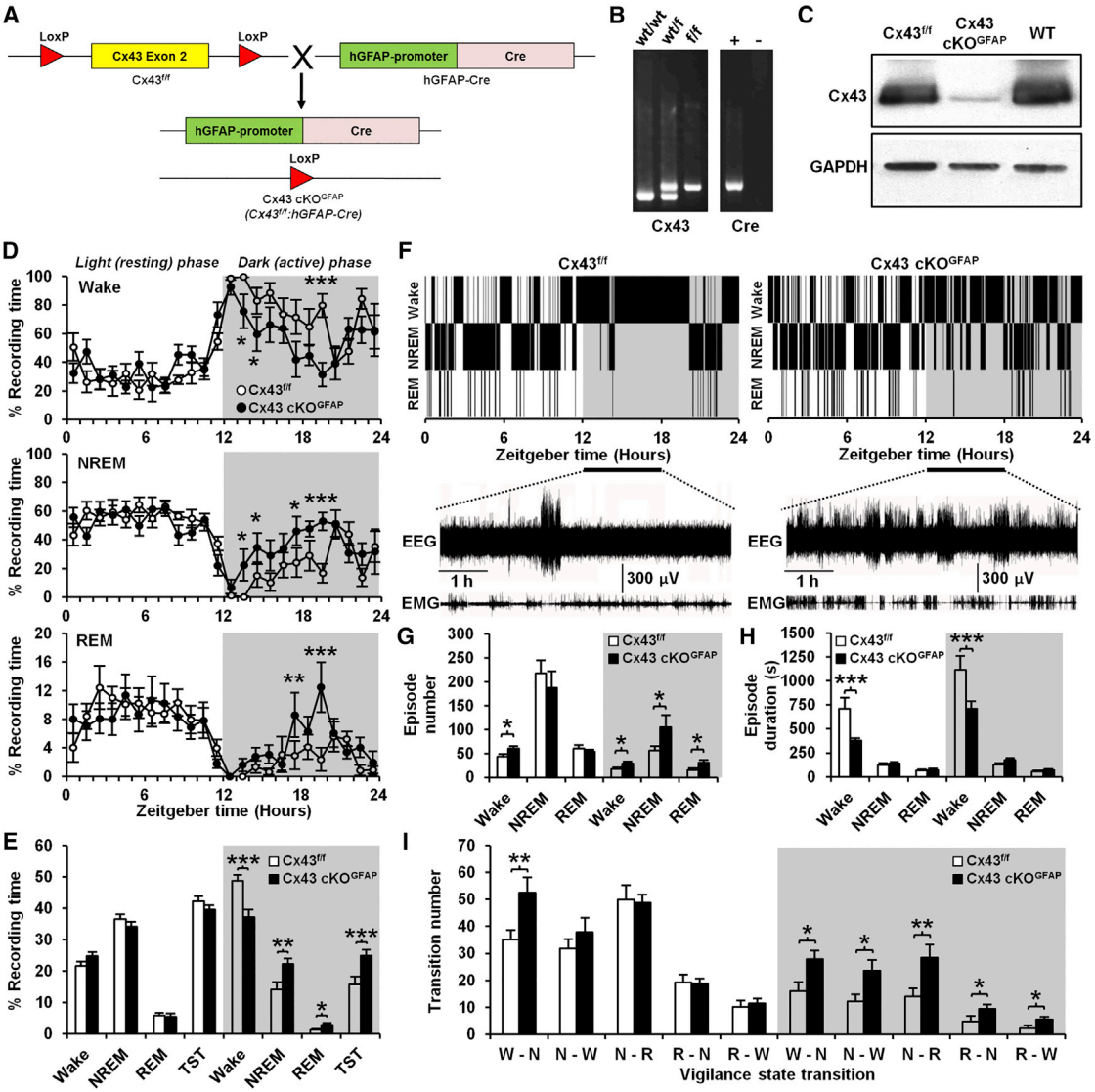

Figure 1. Deletion of Cx43 in Astrocytes Causes Sleepiness and Wakefulness Instability during Active Phase

(A) Generation of mice with conditional knockout of Cx43 in astrocytes.

(B) Left panel: Genotype PCR for the floxed Cx43 allele in wild-type (WT; wt/wt), heterozygous (wt/f), and homozygous (f/f) floxed mice. Right panel: Genotype PCR for GFAP-Cre in Cre-positive mice (+) and Cre-negative littermates (–).

(C) Western blot showing Cx43 expression in whole-brain lysates from Cx43$^{f/f}$, Cx43 cKO^{GFAP}, and WT mice.

(D) Averaged percentage of the time spent in wake (top), NREM (middle), and REM sleep (bottom) per hour in Cx43$^{f/f}$ (n = 8) and Cx43 cKO^{GFAP} mice (n = 7; ANOVA followed by post hoc test; *p < 0.05, **p < 0.01, and ***p < 0.001).

(E) Averaged percentage of time spent in wake, NREM, and REM sleep during the 12 hr light phase and 12 hr dark phase in Cx43$^{f/f}$ (n = 8) and Cx43 cKO^{GFAP} mice (n = 7; ANOVA followed by post hoc test; *p < 0.05, **p < 0.01, and ***p < 0.001). TST, total sleep time including REM and NREM sleep.

(F) Representative hypnograms of Cx43$^{f/f}$ (left) and Cx43 cKO^{GFAP} mice (right). Bottom traces represent EEG/EMG recordings from ZT12 to ZT18.

(G and H) Averages of the number (G) and duration (H) of wake, NREM, and REM sleep episodes during the 12 hr light and dark phases in Cx43$^{f/f}$ (n = 8) and Cx43 cKO^{GFAP} mice (n = 7; ANOVA followed by post hoc test; *p < 0.05 and ***p < 0.001).

(I) Average number of transitions between vigilance states (W, wake; N, NREM; R, REM) in Cx43$^{f/f}$ (n = 8) and Cx43 cKO^{GFAP} mice (n = 7; ANOVA followed by post hoc test; *p < 0.05 and **p < 0.01).

Pooled data are shown as mean ± SEM. See also Figure S1.

hypothesized that the reduced activity of orexin neurons observed in Cx43 cKO^{GFAP} mice could result from a deficiency in the diffusion of energy substrates between astrocytes in the LHA.

To confirm that orexin neurons in Cx43$^{f/f}$ littermate controls use lactate as energy substrate, we used the selective blocker of monocarboxylate transporters (MCTs), α-cyano-4-hydroxy-cinnamate (4-CIN), to block the lactate influx into neuronal cells

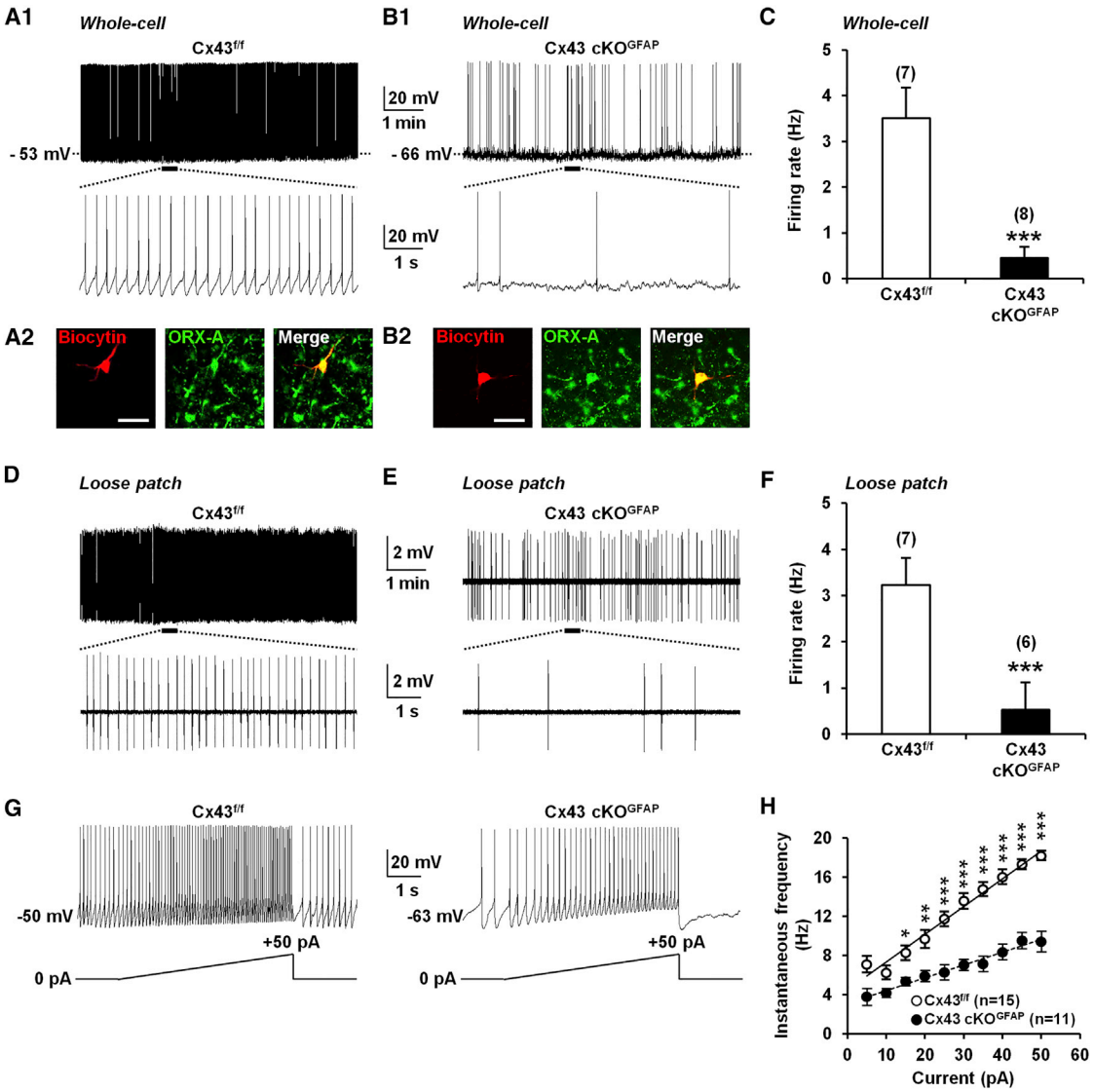

Figure 2. Deletion of Cx43 in Astrocytes Decreases Spontaneous Firing Frequency and Excitability of Orexin Neurons

(A1) Whole-cell current-clamp recording performed in ACSF containing 2.5 mM glucose showing spontaneous tonic firing in an orexin neuron from Cx43$^{f/f}$ mouse. The bottom trace shows an expanded timescale of that recording.

(A2) Images showing the cell recorded in (A1) filled with biocytin (red) and expression of orexin (ORX)-A (green). Scale bar, 50 μm.

(B1 and B2) Same experiments as in (A1) and (A2) but in an orexin neuron from Cx43 cKO^{GFAP} mouse.

(C) Average firing rate of orexin neurons recorded from Cx43$^{f/f}$ (n = 7 cells, 5 mice) and Cx43 cKO^{GFAP} mice (n = 8 cells, 4 mice; Mann-Whitney test, ***$p < 0.001$) recorded in the whole-cell current-clamp mode.

(D) Loose patch-clamp recording of spontaneous firing in an orexin neuron from Cx43$^{f/f}$ mouse.

(E) Same experiment as in (D) but in an orexin neuron from a Cx43 cKO^{GFAP} mouse.

(F) Average firing rate of orexin neurons recorded from Cx43$^{f/f}$ (n = 7 cells, 4 mice) and Cx43 cKO^{GFAP} mice (n = 6 cells, 3 mice; Mann-Whitney test, ***$p < 0.001$) in loose patch-clamp configuration.

(G) Whole-cell current-clamp recordings performed in ACSF containing 2.5 mM glucose showing the membrane response of an orexin neuron from Cx43$^{f/f}$ (left) and Cx43 cKO^{GFAP} mice (right) to a positive current ramp from 0 to 50 pA (5 s).

(H) Average instantaneous frequency of orexin neurons from Cx43$^{f/f}$ (n = 15 cells, 9 mice) and Cx43 cKO^{GFAP} mice (n = 11 cells, 7 mice; ANOVA followed by post hoc test; *$p < 0.05$, **$p < 0.01$, ***$p < 0.001$) in 5 pA bins during the incremental current injection.

Pooled data are shown as mean ± SEM. See also Figure S2.

(Parsons and Hirasawa, 2010). In the presence of physiological levels of glucose (2.5 mM), bath application of 4-CIN (500 μM) induced a reversible membrane hyperpolarization of 9.71 ± 1.47 mV (n = 7 cells, 3 mice) that was sufficient to inhibit the tonic firing of orexin neurons (Figures 3A and 3B). To test whether exogenous lactate was sufficient to sustain the activity of orexin

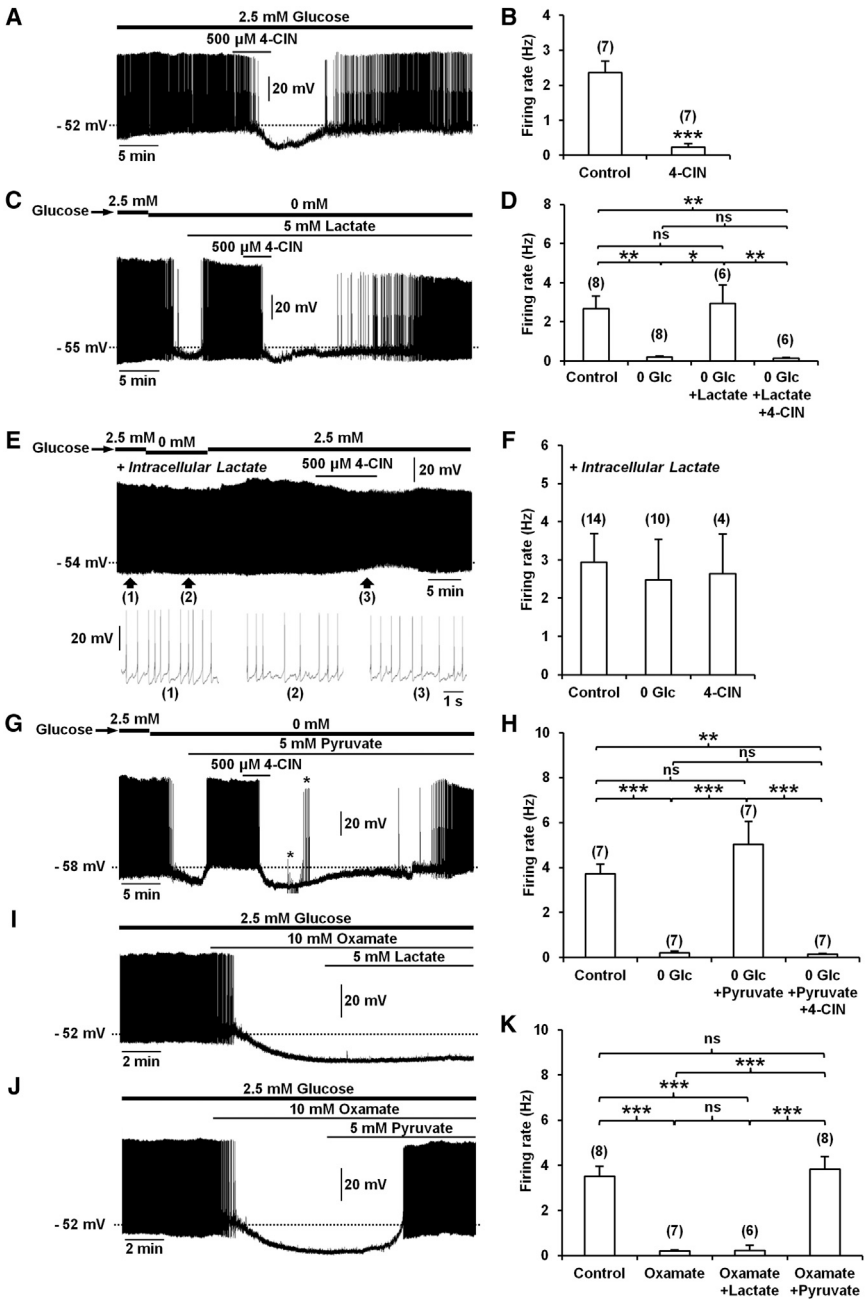

Figure 3. Endogenous Production of Lactate Sustains Spontaneous Activity of Orexin Neurons

(A) Whole-cell current-clamp recording performed in ACSF containing 2.5 mM glucose showing that bath application of the MCT inhibitor 4-CIN hyperpolarized and decreased the firing rate of an orexin neuron from a Cx43$^{f/f}$ mouse.

(B) Summary of the 4-CIN effect on the firing rate of orexin neurons from Cx43$^{f/f}$ mice (n = 7 cells, 3 mice; paired Student's t test; ***p < 0.001).

(C) Whole-cell current-clamp recording showing that a switch from 2.5 to 0 mM glucose hyperpolarized and decreased the firing rate of an orexin neuron from a Cx43$^{f/f}$ mouse. On the same neuron, lactate reversed the glucose deprivation effect, and this effect was cancelled by 4-CIN.

(D) Average firing rate of orexin neurons from Cx43$^{f/f}$ mice in different conditions (in 2.5 mM glucose [Control], n = 8 cells, 6 mice; in 0 mM glucose [0 Glc], n = 8 cells, 6 mice; in 0 mM glucose with lactate, n = 6 cells, 3 mice; in 0 mM glucose with lactate and 4-CIN, n = 6 cells, 3 mice; ANOVA followed by post hoc test; *p < 0.05 and **p < 0.01; ns, nonsignificant).

(E) Intracellular dialysis of 2.5 mM lactate (> 20 min) in an orexin neuron from a Cx43$^{f/f}$ mouse through the patch pipette prevented the inhibitory effects of glucose deprivation and 4-CIN. Bottom traces show expanded timescales of the recording at the indicated time points 1, 2, and 3.

(F) Average firing rate of orexin neurons from Cx43$^{f/f}$ mice during intracellular dialysis of 2.5 mM lactate in 2.5 mM glucose (Control, n = 14 cells, 8 mice), 0 mM glucose (0 Glc, n = 10 cells, 6 mice), and 2.5 mM glucose with 4-CIN (4-CIN, n = 4 cells, 3 mice; ANOVA, p > 0.05).

(G) Whole-cell current-clamp recording of an orexin neuron from a Cx43$^{f/f}$ mouse showing that bath application of the downstream metabolite of LDH, pyruvate, reversed the inhibitory effect of glucose deprivation. The pyruvate effect was suppressed by 4-CIN. Asterisks indicate the time of application of hyperpolarizing and depolarizing current pulses to trace current-voltage relationships.

(H) Average firing rate of orexin neurons from Cx43$^{f/f}$ mice in different conditions (in 2.5 mM glucose [Control]; in 0 mM glucose [0 Glc]; in 0 mM glucose with pyruvate; in 0 mM glucose with pyruvate and 4-CIN; n = 7 cells, 3 mice for each condition; ANOVA followed by post hoc test; **p < 0.01 and ***p < 0.001; ns, nonsignificant).

(I) Whole-cell current-clamp recording showing that the LDH inhibitor oxamate hyperpolarized and decreased the firing rate of an orexin neuron from a Cx43$^{f/f}$ mouse in ACSF with 2.5 mM glucose. On the same neuron, lactate, the upstream substrate of LDH, did not reverse the inhibitory effect of oxamate.

(J) Whole-cell current-clamp recording of an orexin neuron from a Cx43$^{f/f}$ mouse showing that pyruvate reversed the inhibitory effect of oxamate.

(K) Average firing rate of orexin neurons from Cx43$^{f/f}$ mice in different conditions (in 2.5 mM glucose [Control], n = 8 cells, 3 mice; in 2.5 mM glucose with oxamate [Oxamate], n = 7 cells, 3 mice; in 2.5 mM glucose with oxamate and lactate [Oxamate + Lactate], n = 6 cells, 3 mice; in 2.5 mM glucose with oxamate and pyruvate [Oxamate + Pyruvate], n = 8 cells, 3 mice; ANOVA followed by post hoc test; ***p < 0.001; ns, nonsignificant).

Pooled data are shown as mean ± SEM. See also Figure S3.

neurons, we induced glucose deprivation by switching from 2.5 to 0 mM glucose in ACSF. This caused a membrane hyperpolarization (from −55.25 ± 1.69 mV to −66.37 ± 1.98 mV, n = 8 cells, 6 mice; paired Student's t test, p < 0.001) that was sufficient to inhibit the activity of orexin neurons (Figures 3C and 3D). During glucose deprivation, bath application of 5 mM lactate (equicaloric to 2.5 mM glucose; Parsons and Hirasawa, 2010) restored both the basal membrane potential (−54.50 ± 2.37 mV, n = 6 cells, 3 mice; Student's t test, p > 0.05) and spontaneous firing frequency of orexin neurons (Figures 3C and 3D). The recovering

effect of lactate on orexin neuron activity during glucose deprivation was abrogated when slices were perfused with 500 μM 4-CIN (Figures 3C and 3D), suggesting that the excitatory effect of lactate required its transport through the cell membrane. The requirement for lactate being transported into the neuron, rather than acting on an extracellular receptor (Tang et al., 2014), was confirmed by performing additional recordings with a patch pipette solution containing lactate under conditions of energy depletion. Dialysis of orexin neurons with 2.5 mM lactate in whole-cell configuration for 20–30 min after break-in prevented the inhibitory effects of either glucose deprivation or 4-CIN (Figures 3E and 3F). Together, these data suggest that orexin neuronal activity is primarily dependent on lactate uptake.

Based on the ANLS hypothesis, lactate produced from astrocytic glucose and taken up by neurons via MCTs mediates its effect through lactate dehydrogenase (LDH), an enzyme responsible for conversion of lactate to pyruvate, the downstream metabolite that enters the tricarboxylic cycle to fuel neurons (Pellerin and Magistretti, 1994; Bélanger et al., 2011; Lam et al., 2005; Sada et al., 2015). In favor of this hypothesis, we found that bath application of pyruvate (5 mM), which can also be transported into the cells by MCTs (Halestrap and Price, 1999), rescued the inhibitory effect of glucose deprivation on orexin neurons, an action that was suppressed by 500 μM 4-CIN (Figures 3G and 3H). Also, inhibition of LDH by bath application of 10 mM oxamate (Sada et al., 2015), to prevent the conversion of lactate to pyruvate, hyperpolarized orexin neurons (from −54.42 ± 1.75 mV to −67.14 ± 1.38 mV, n = 7 cells, 3 mice; paired Student's t test, $p < 0.001$) and strongly suppressed their spike firing (Figures 3I–3K), mimicking the inhibitory effect of glucose deprivation (Figures 3C, 3D, 3G, and 3H). Finally, membrane hyperpolarization and loss of activity induced by oxamate were both fully restored by bath application of pyruvate (5 mM), the downstream metabolite of LDH (membrane potential in the presence of oxamate + pyruvate, −52.00 ± 1.43 mV, n = 8 cells, 3 mice; Student's t test, $p > 0.05$; Figures 3J and 3K), but not by the addition of lactate (5 mM), the upstream substrate of LDH (membrane potential in presence of oxamate + lactate, −66.16 ± 2.32 mV, n = 6 cells, 3 mice; Student's t test, $p < 0.01$; Figures 3I and 3K). These results indicate that lactate mediates its excitatory effects on orexin neurons through the activity of the LDH enzyme, a metabolic component of the ANLS.

What is the mechanism for the effect of lactate on membrane potential and spontaneous tonic firing of orexin neurons? We found that the membrane hyperpolarization induced by glucose deprivation (from −47.33 ± 3.38 mV to −61.67 ± 5.36 mV, n = 3 cells, 3 mice; paired Student's t test, $p < 0.05$) persisted under 0.5 μM tetrodotoxin (Figure S3A), suggesting a direct postsynaptic effect. The membrane hyperpolarization was caused by activation of a current that reversed near the potassium equilibrium potential (−83.38 ± 8.18 mV, n = 4 cells, 3 mice; Figures S3B1 and S3B2). We next observed that the inhibitory effect of glucose deprivation was either restored (Figures S3C and S3D) or prevented (Figures S3E and S3G) by bath application of tolbutamide (100 μM), a blocker of ATP-sensitive potassium (K_{ATP}) channels (Sada et al., 2015), suggesting that K_{ATP} channels mediated the inhibition of orexin neurons. To confirm that maintenance of orexin neuron activity by lactate, and to some extent by pyruvate, involves K_{ATP} channels, we tested the effect of tolbutamide on 4-CIN- and oxamate-induced inhibition of orexin neurons. Pre-treatment of slices with tolbutamide (100 μM) for at least 15 min completely abolished the inhibitory effect caused by 500 μM 4-CIN and 10 mM oxamate (Figures S3E–S3G). Consistent with previous studies (Parsons and Hirasawa, 2010), these results indicate that lactate sustains tonic spontaneous activity of orexin neurons by modulating K_{ATP} channel activity.

We asked whether the delivery of lactate into a single astrocyte in the LHA could rescue normal activity of orexin neurons during glucose deprivation. A single astrocyte was dialyzed with 5 mM lactate while performing whole-cell recording from a distant orexin neuron (50–75 μm apart; Figures 4A and 4B). When astrocytes were dialyzed with lactate, glucose deprivation no longer induced a reduction in AP firing nor a membrane hyperpolarization (Figures 4C–4F). This preventive effect of lactate was suppressed by 4-CIN (500 μM; Figures 4D–4F), indicating that transcellular transport of lactate through MCTs was required for its effect. These data show that shuttling of lactate from astrocytes to neurons is functional in the LHA and contributes to the tonic firing of orexin neurons.

Gap Junction-Mediated Astrocytic Networks Are Functional in the LHA

Gap junction-mediated astrocytic networks are functional in the LHA, since injection of biocytin (Rouach et al., 2008) into a single astrocyte diffused from the patch pipette extensively into neighboring astrocytes (Figures 5A and 5D). This intercellular diffusion was significantly attenuated by the gap junction blocker, carbenoxolone (CBX; 50 μM; Rouach et al., 2008; Figures 5C and 5D). Most coupled cells were immunopositive for the astrocyte marker GFAP, but not for the neuronal marker NeuN (Figure 5E), suggesting a lack of dye-coupling between astrocytes and neurons in the LHA. When orexin neurons were recorded, biocytin was always restricted to the recorded cell (Figures 2A2 and 2B2), showing a lack of intercellular communication between astrocytes and orexin neurons. Together, these results demonstrate functional gap junctional coupling between astrocytes surrounding orexin neurons in the LHA.

We next studied the possibility for energy metabolites to traffic between astrocytes in the LHA by injecting the fluorescent glucose derivative 2-[N-(7-nitrobenz-2-oxa-1,3-diazol-4-yl)amino]-2-deoxyglucose (2-NBDG; Rouach et al., 2008) into a single LHA astrocyte via a patch pipette and analyzing its intercellular diffusion. Twenty minutes after break-in, 2-NBDG diffused from the patch pipette into neighboring astrocytes (Figures 5F and 5H).

Cx43 Deletion in Astrocytes Weakens the Astrocytic Metabolic Networks in the LHA

We next investigated by whole-cell recordings whether gap junctional coupling and trafficking of energy metabolites between astrocytes were altered in the LHA of Cx43 cKO^{GFAP}. Passive membrane properties of LHA astrocytes were similar between Cx43 cKO^{GFAP} and $Cx43^{f/f}$ mice (Figure S4). However, the

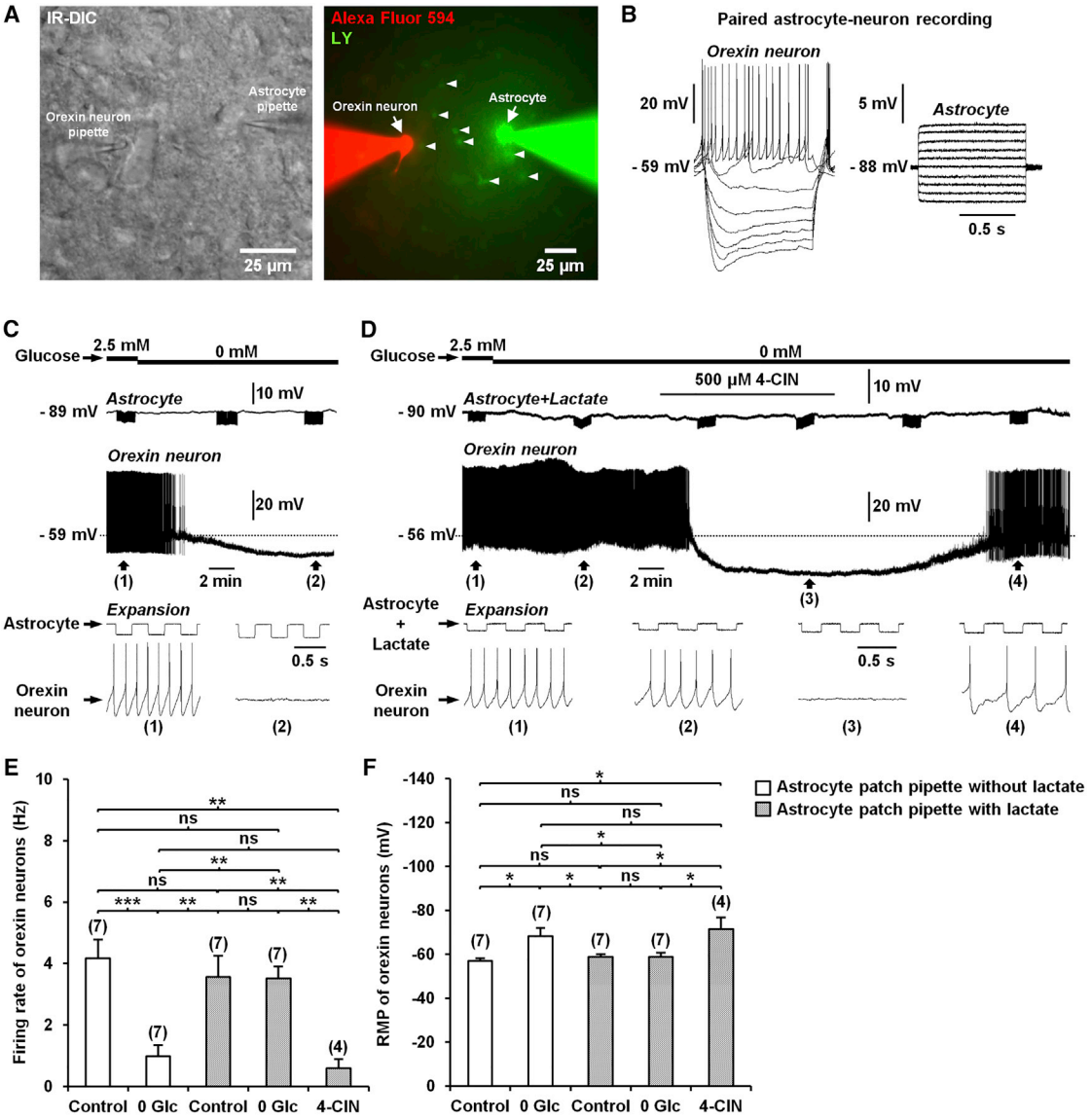

Figure 4. Lactate Supply through the Astrocytic Network Sustains the Activity of Orexin Neurons during Glucose Deprivation

(A) Left: Infrared differential interference contrast (IR-DIC) image of a paired astrocyte-orexin neuron whole-cell recording in the LHA from a Cx43$^{f/f}$ mouse. Right: Fluorescence image of the orexin neuron-astrocyte pair shown in the left picture, filled through the pipette with Alexa Fluor 594 (red) and Lucifer yellow (LY, green), respectively. Note the diffusion of LY to neighboring astrocytes (arrowheads).

(B) Responses of the cells recorded in (A) to current pulses from −60 to 10 pA (1 s, 10 pA steps) for the orexin neuron and from −200 to 250 pA (1 s, 50 pA steps) for the astrocyte.

(C) Representative paired astrocyte-neuron recording from a Cx43$^{f/f}$ mouse showing that glucose deprivation inhibits the orexin neuron firing rate. Downward deflections in the astrocyte trace are membrane potential responses to current pulses (−100 pA at 2 Hz for 80 s) to monitor input resistance.

(D) Intracellular delivery of lactate (5 mM) to astrocyte (Astrocyte + Lactate) through the patch pipette for at least 20 min prevents the inhibitory effect of glucose deprivation on the orexin neuron firing rate. This preventive effect was abolished by bath application of 4-CIN.

(E and F) Average firing frequency (E) and resting membrane potential (RMP; F) of orexin neurons from Cx43$^{f/f}$ mice exposed to different conditions (during patch-clamp recording of astrocyte not filled with lactate: in 2.5 mM glucose [Control], n = 7 cells, 5 mice; in 0 mM glucose [0 Glc], n = 7 cells, 5 mice; during patch-clamp recording of astrocyte filled with 5 mM lactate: in 2.5 mM glucose [Control], n = 7 cells, 4 mice; in 0 mM glucose [0 Glc], n = 7 cells, 4 mice; in 500 µM 4-CIN, n = 4 cells, 4 mice; ANOVA followed by post hoc test; *p < 0.05, **p < 0.01, and ***p < 0.001; ns, nonsignificant).

Pooled data are shown as mean ± SEM.

number of dye-coupled LHA astrocytes following biocytin injection was reduced by 54.63% in Cx43 cKO^{GFAP} (Figures 5A, 5B, and 5D). Similarly, the intercellular diffusion of 2-NBDG between LHA astrocytes was decreased by 52.12% in the cKO animals (Figures 5F–5H), indicating that glucose trafficking through the astrocytic network in the LHA requires Cx43.

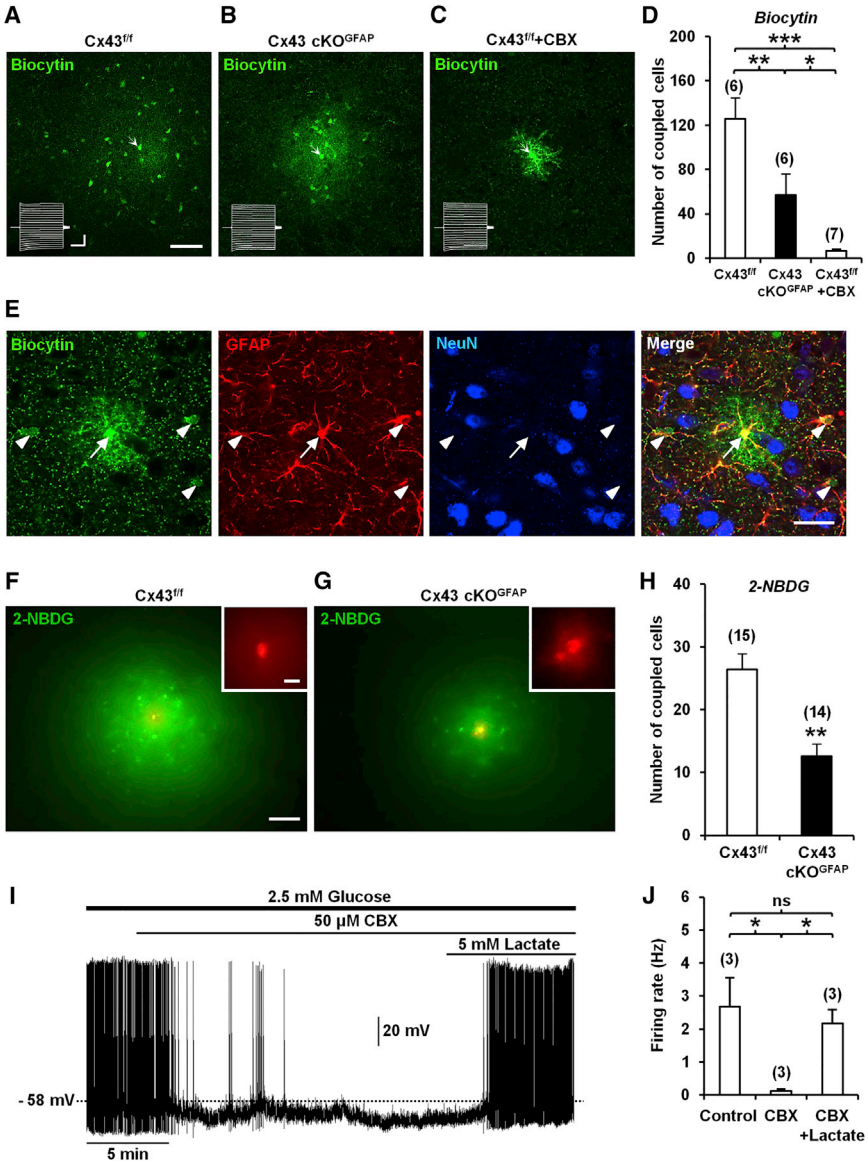

Figure 5. Deletion of Cx43 in Astrocytes Alters Metabolic Networks of Interconnected Astrocytes in the LHA

(A) Functional coupling of astrocytes in the LHA from a Cx43$^{f/f}$ mouse observed by injection of biocytin (20 min, green) in a single astrocyte (arrow) through the patch pipette. Biocytin diffusion was revealed with streptavidin after slice fixation. Scale bar, 50 µm. Inset shows current traces in the patched astrocyte (arrow) while holding membrane potential at −80 mV in response to a series of voltage pulses from −100 to +100 mV (300 ms, 10 mV steps). Calibration bars, 4 nA, 100 ms.

(B) Same experiment as in (A) but in an orexin neuron from a Cx43 cKO^{GFAP} mouse.

(C) Treatment of slices from Cx43$^{f/f}$ mice with the gap junction channel blocker carbenoxolone (CBX, 50 µM, > 15 min) abolished intercellular diffusion of biocytin (green) between LHA astrocytes, revealing fine astrocytic processes.

(D) Summary of the number of coupled cells recorded in Cx43$^{f/f}$ (n = 6, 2 mice), Cx43 cKO^{GFAP} (n = 6, 3 mice), and Cx43$^{f/f}$ slices treated with CBX (Cx43$^{f/f}$ + CBX, n = 7, 2 mice; ANOVA followed by post hoc test; *p < 0.05, **p < 0.01, and ***p < 0.001).

(E) Dye coupling of LHA astrocytes from a Cx43$^{f/f}$ mouse performed with biocytin (green) injected in a single astrocyte (arrow) through the patch pipette and combined with a double immunofluorescence staining for GFAP (red) and NeuN (blue). Scale bar, 50 µm.

(F) Spread through astrocytic network of the fluorescent glucose analog 2-NBDG (green) injected in a single LHA astrocyte from a Cx43$^{f/f}$ mouse through the patch pipette (20 min). Scale bar, 100 µm. The injected astrocyte was localized by simultaneously injecting the gap junction-impermeable dye dextran tetramethylrhodamine (red, inset). Scale bar, 10 µm.

(G) Same experiment as in (F) but in a Cx43 cKO^{GFAP} mouse.

(H) Summary of the extent of astrocytic coupling in the LHA for the 2-NBDG in Cx43$^{f/f}$ (n = 15 slices, 5 mice) and Cx43 cKO^{GFAP} mice (n = 14 slices, 4 mice; Mann-Whitney test; **p < 0.01).

(I) Whole-cell current-clamp recording showing that CBX hyperpolarized and decreased the firing rate of an orexin neuron from a Cx43$^{f/f}$ mouse bathed in ACSF with 2.5 mM glucose. On the same neuron, addition of lactate reversed the inhibitory effect of CBX.

(J) Average firing rate of orexin neurons from Cx43$^{f/f}$ mice in different conditions (in 2.5 mM glucose [Control], in 2.5 mM glucose with CBX [CBX], in 2.5 mM glucose with CBX and lactate [CBX + Lactate]; n = 3 cells, 3 mice for each condition; ANOVA; *p < 0.05; ns, nonsignificant).

Pooled data are shown as mean ± SEM. See also Figure S4.

Exogenous Lactate Restores the Activity of Orexin Neurons in Cx43 cKO^{GFAP} Mice

Given that orexin neuron activity relies on lactate, we asked whether exogenous lactate could restore the activity of these cells in Cx43 cKO^{GFAP} mice. In Cx43 cKO^{GFAP}, bath application of 5 mM lactate in the presence of 2.5 mM glucose induced a membrane depolarization of 8.50 ± 1.11 mV (n = 8 cells, 4 mice) that was sufficient to restore the spontaneous activity of orexin neurons (Figures 6B and 6C). The recovery of spike firing by lactate was preserved during loose patch recordings (Figures 6E and 6F). Under the same treatment, the reduced excitability of orexin neurons in Cx43 cKO^{GFAP} mice also recovered and reached the level of that of orexin neurons from Cx43$^{f/f}$ mice (Cx43 cKO^{GFAP} + lactate, 0.26 ± 0.03 Hz/pA, n = 7 cells, 3 mice; Cx43$^{f/f}$, 0.29 ± 0.03 Hz/pA, n = 9 cells, 4 mice; Student's t test, p > 0.05; Figures 6G–6J). Moreover, in orexin neurons from Cx43$^{f/f}$ mice, exogenous delivery of lactate (5 mM) in the presence of 2.5 mM glucose had no effect on the membrane potential (without lactate, −47.57 ± 1.52 mV; with lactate, −47.00 ± 1.41 mV; n = 7 cells, 3 mice for each condition; paired Student's t test, p > 0.05; Figure 6A), spike frequency firing (Figures 6A, 6C, 6D, and 6F), and cell excitability (without lactate, 0.29 ± 0.03 Hz/pA, n = 9 cells, 4 mice; with lactate, 0.28 ± 0.03 Hz/pA, n = 9 cells, 5 mice; Student's t test, p > 0.05;

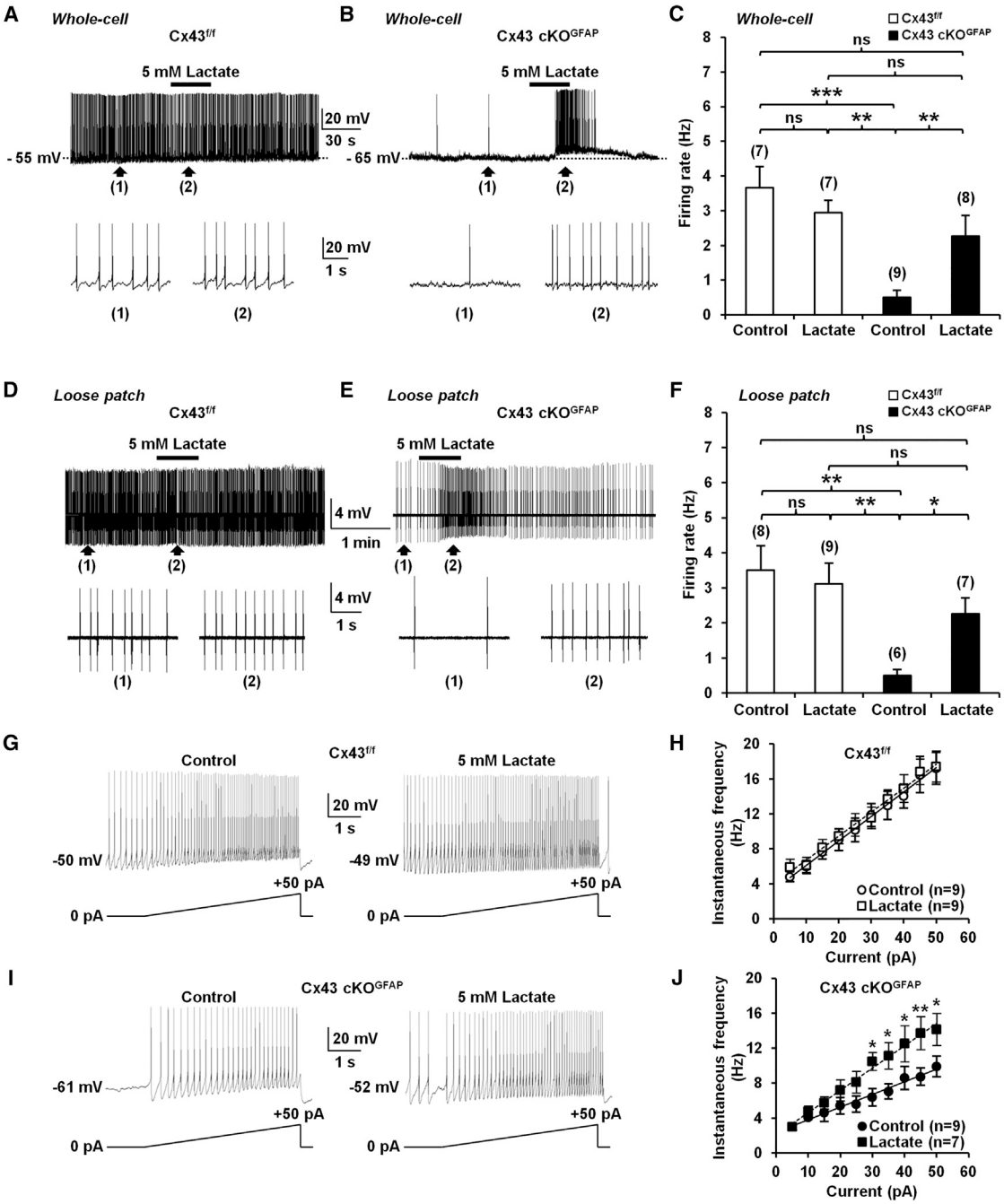

Figure 6. Lactate Restores Spontaneous Firing Frequency and Excitability of Orexin Neurons from Cx43 cKO^{GFAP} Mice

(A) Whole-cell current-clamp recording showing that bath application of 5 mM lactate (equicaloric to 2.5 mM glucose) had no effect on the membrane potential and firing rate of an orexin neuron from a Cx43$^{f/f}$ mouse bathed in ACSF with 2.5 mM glucose.

(B) Same experiment as in (A) showing that lactate depolarized and accelerated the firing rate of an orexin neuron from a Cx43 cKO^{GFAP} mouse.

(C) Average firing rate of orexin neurons recorded in whole-cell current-clamp mode while bathed in ACSF with 2.5 mM glucose in the presence and absence of lactate among genotypes (Cx43$^{f/f}$ without lactate [Control], n = 7 cells, 4 mice; Cx43$^{f/f}$ with lactate, n = 7 cells, 3 mice; Cx43 cKO^{GFAP} without lactate [Control], n = 9 cells, 4 mice; Cx43 cKO^{GFAP} with lactate, n = 8 cells, 4 mice; ANOVA followed by post hoc test; $^{**}p < 0.01$ and $^{***}p < 0.001$; ns, nonsignificant).

(D) Loose patch-clamp recording showing that lactate did not have any effect on the firing of an orexin neuron from a Cx43$^{f/f}$ mouse in ACSF with 2.5 mM glucose.

(E) Same experiment as in (D) showing that lactate increased firing frequency of an orexin neuron from a Cx43 cKO^{GFAP} mouse.

(F) Average firing rate of orexin neurons recorded in loose patch configuration in different genotypes and conditions (Cx43$^{f/f}$ without lactate [Control], n = 8 cells, 4 mice; Cx43$^{f/f}$ with lactate, n = 9 cells, 4 mice; Cx43 cKO^{GFAP} without lactate [Control], n = 6 cells, 3 mice; Cx43 cKO^{GFAP} with lactate, n = 7 cells, 3 mice; ANOVA followed by post hoc test; $^{*}p < 0.05$ and $^{**}p < 0.01$; ns, nonsignificant).

(legend continued on next page)

Figures 6G and 6H). These results suggest that the decreased activity of orexin neurons in Cx43 cKO^{GFAP} results from a deficiency in the trafficking of glucose-derived lactate through the astrocytic network. Furthermore, pharmacological inhibition of the gap junction network with 50 μM CBX in brain slices from Cx43$^{f/f}$ mice phenocopied those from Cx43 cKO^{GFAP} mice with reduced activity of orexin neurons (Figures 5I and 5J), which was recovered by exogenous supply of 5 mM lactate (Figures 5I and 5J).

In Vivo Knockout of Cx43 in LHA Astrocytes Causes Excessive Sleepiness and Fragmented Wakefulness during the Active Phase

To determine whether the sleep-wake phenotype observed in Cx43 cKO^{GFAP} mice was specific to LHA astrocytes, we performed cortical EEG/EMG recordings in Cx43$^{f/f}$ mice bilaterally injected in the LHA with an AAV vector of serotype 8 carrying the construct hGfa2-Cre:GFP in which Cre recombinase, fused to green fluorescent protein (GFP; Matsuda and Cepko, 2007), is under the control of an astrocyte-selective human hGfa2 promoter (Brenner et al., 1994; Lee et al., 2008), which is a truncated version of the GFAP promoter (Figure 7A). Three weeks after transduction of Cx43$^{f/f}$ mice with AAV, we observed efficient and selective expression of Cre:GFP in LHA astrocytes (Figures 7B, S5A, and S5B). Out of 967 total GFP-expressing cells in the targeted LHA of transduced mice, 700 cells were positive for GFAP (72.38%, n = 4; Figures S5A and S5B) and none were positive for ORX-A or NeuN (Figures S5A and S5B). Cortical EEG/EMG electrodes were implanted in transduced animals 10 days after the injection. EEG/EMG recordings started 4 days later for up to 7 days. On day 21 post-injection, sleep-wake parameters were compared with those of two different control groups of mice (Figure 7A): (1) Cx43$^{f/f}$ mice injected bilaterally in the LHA with ACSF vehicle (n = 4) and (2) WT mice bearing the same C57BL/6J inbred background injected bilaterally in the LHA with AAV-hGfa2-Cre:GFP (n = 4). Since the baseline 24 hr sleep-wake distribution (Figures S5C and S5D), the number and duration of vigilance-state episodes (Figures S5E and S5F), and their number of transitions (Figure S5G) were similar in both control groups, we pooled them together as one control group. Compared with control mice, Cx43$^{f/f}$ mice transduced with AAV showed a decrease in time spent awake during the dark phase concomitant with an increase in the time spent in NREM sleep and TST (Figures 7C and 7D). In AAV-transduced Cx43$^{f/f}$ mice, wake episodes were frequently interrupted by short episodes of NREM sleep during the beginning of the dark phase from ZT12 to ZT18 (Figures 7E). These animals exhibited more wake episodes of shorter duration than controls (Figures 7F and 7G). The number of NREM sleep episodes was also increased in AAV-transduced Cx43$^{f/f}$ mice during the dark phase (Figure 7F), but without a change in their duration (Figure 7G). This nocturnal fragmented wakefulness was associated with an increase in the number of transitions from wake to NREM as well as from NREM to wake (Figure 7H). Thus, these data demonstrate that selective knockout of Cx43 in LHA astrocytes caused excessive sleepiness and instability of wakefulness during the nocturnal active phase, phenocopying the Cx43 cKO^{GFAP} mice.

Lactate Delivery Counteracts Nocturnal Wakefulness Instability Induced in Cx43$^{f/f}$ Mice by the Injection of AAV-hGfa2-Cre:GFP in the LHA

We asked whether in vivo delivery of lactate to the LHA would rescue the wakefulness instability induced in Cx43$^{f/f}$ mice by the transduction with AAV-hGfa2-Cre:GFP. We used osmotic minipumps to bilaterally introduce ACSF vehicle and subsequently lactate (5 mM) in the LHA of the same individual Cx43$^{f/f}$ mice after implantation of cortical EEG/EMG electrodes and AAV transduction (Figure 8A). Twenty-one days after AAV-hGfa2-Cre:GFP injection, Cx43$^{f/f}$ mice showed a change in the sleep-wake distribution characterized by a significant decrease in the time spent awake during the first 6 hr of the dark phase from ZT12 to ZT18 (Figures 8B and 8C), which was concomitant with a significant increase in the time spent in NREM sleep (Figures 8B and 8C) and TST (Figure 8C). This was accompanied by fragmented wakefulness (Figure 8D) characterized by increased number of wake episodes (Figure 8E) that were shorter in duration (Figure 8F). Transition numbers from wake to NREM and from NREM to wake were also increased after AAV transduction (Figure 8G). While chronic infusion of ACSF for 1 week did not affect sleep-wake parameters in these animals (Figures 8B–8G), subsequent treatment with lactate for the same duration fully reversed the effects of AAV transduction by restoring the sleep-wake distribution (Figures 8B and 8C), the number and duration of wake and NREM sleep episodes (Figures 8D–8F), and the number of transitions between wake and NREM sleep (Figure 8G). Thus, these results demonstrate that chronic in vivo delivery of lactate ameliorates nocturnal wakefulness instability induced by the loss of astroglial Cx43 in the LHA by restoring sustained wakefulness.

DISCUSSION

Our results reveal an important role for astroglial Cx43 in sleep-wake regulation. We demonstrate that conditional deletion of Cx43 in astrocytes causes changes in sleep/wake patterns with disturbances of sleep and wakefulness. We found that Cx43 cKO^{GFAP} mice have reduced wakefulness concomitant

(G) Whole-cell current-clamp recording in ACSF with 2.5 mM glucose showing the membrane response of an orexin neuron from a Cx43$^{f/f}$ mouse to a positive current ramp from 0 pA to 50 pA (5 s) in the absence (Control, left) or presence (right) of lactate.
(H) Average instantaneous frequency of orexin neurons from Cx43$^{f/f}$ mice in 5 pA bins during the incremental current injection in the absence (Control, n = 9 cells, 4 mice) or presence of lactate (n = 9 cells, 5 mice; ANOVA; $p > 0.05$).
(I) Same experiments as in (G) showing that lactate increased excitability of an orexin neuron from a Cx43 cKO^{GFAP} mouse.
(J) Average instantaneous frequency of orexin neurons from Cx43 cKO^{GFAP} mice in 5 pA bins during the incremental current injection in the absence (Control, n = 9 cells, 4 mice) or presence of lactate (n = 7 cells, 3 mice; ANOVA followed by post hoc test; $^{*}p < 0.05$ and $^{**}p < 0.01$).
Pooled data are shown as mean ± SEM.

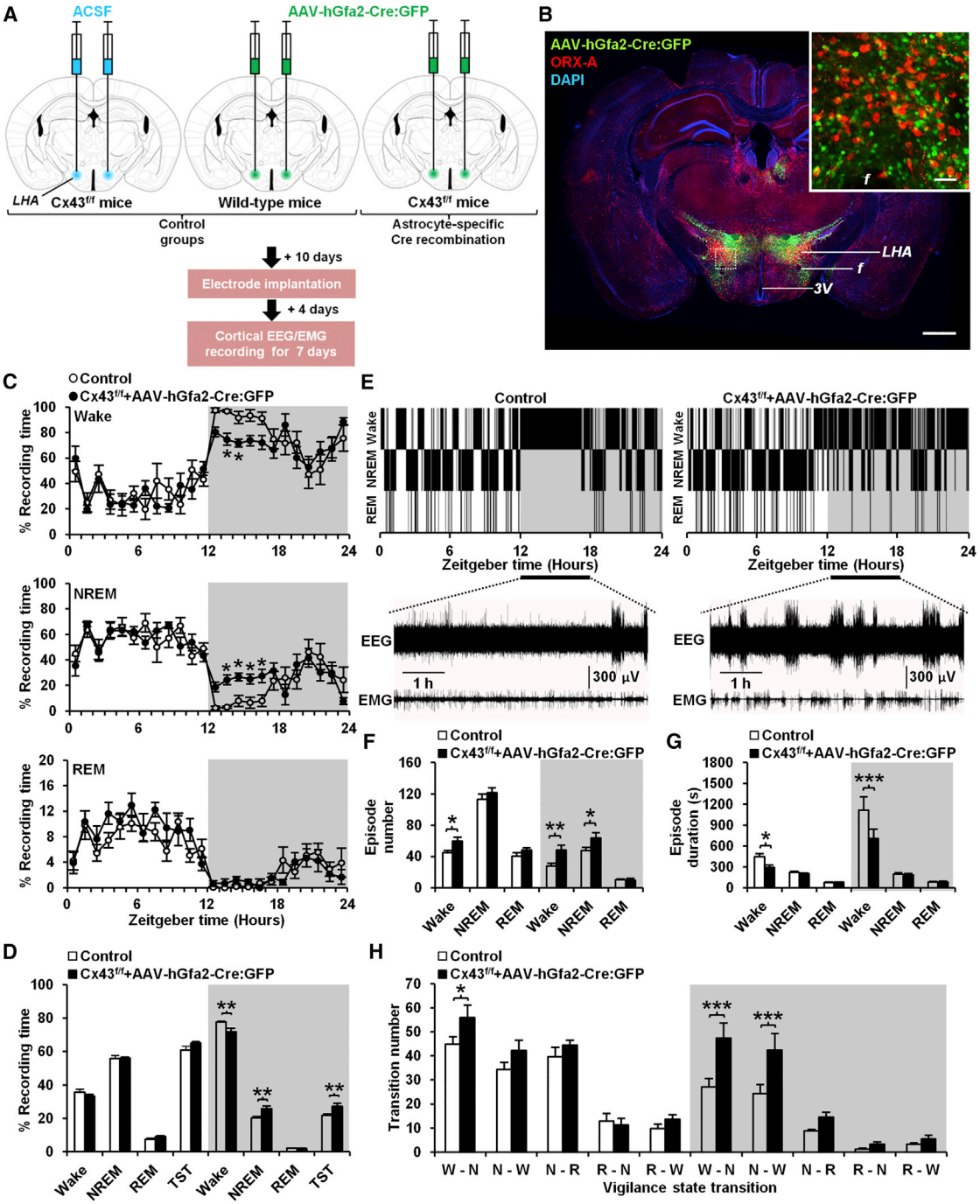

Figure 7. Deletion of Cx43 in Astrocytes from the LHA Causes Sleepiness and Instability of Wakefulness during the Nocturnal Active Phase

(A) Experimental design and timeline.

(B) Brain section from a Cx43$^{f/f}$ mouse 21 days after bilateral injection of AAV-hGfa2-Cre:GFP into the LHA showing Cre:GFP expression (green), ORX-A-immunopositive cells (red), and DAPI nuclear staining (blue). f, fornix; LHA, lateral hypothalamic area; 3V, third ventricle. Scale bar, 500 µm. The inset represents a magnification of the area delimited by the dash rectangle. Scale bar, 50 µm.

(C) Percentage average of the time spent in wake (top), NREM sleep (middle), and REM sleep (bottom) per hour in control (n = 8) and Cx43$^{f/f}$ mice transduced with AAV 21 days after injections (Cx43$^{f/f}$ + AAV-hGfa2-Cre:GFP, n = 8; wake and NREM sleep: ANOVA followed by post hoc test, *p < 0.05; REM sleep: ANOVA, p > 0.05).

(D) Averaged percentage of time spent in wake, NREM, and REM sleep during the 12 hr light and dark phases in control (n = 8) and Cx43$^{f/f}$ mice transduced with AAV (n = 8; ANOVA followed by post hoc test; **p < 0.01). TST, total sleep time including REM and NREM sleep.

(legend continued on next page)

with increased NREM sleep during the dark phase, at a time when mice, as nocturnal animals, would normally spend more time awake. Wakefulness in these animals was fragmented, frequently interrupted by short periods of NREM sleep. Consequently, Cx43 cKO^{GFAP} mice had increased episode numbers for wake and NREM sleep and more frequent transitions from wake to sleep states and vice versa. These results reveal that Cx43 cKO^{GFAP} mice were unable to maintain persistent wakefulness during the normal wake phase.

Excessive sleepiness and instability in wakefulness may be a consequence of altered control of arousal-related brain regions. It is known that the LHA, which contains orexin neurons, plays a critical role in arousal stability (Sakurai, 2007). Notably, orexin deficiency has been linked to the chronic sleep disorder narcolepsy in animals (Lin et al., 1999; Chemelli et al., 1999; Willie et al., 2003; Mochizuki et al., 2004; Tabuchi et al., 2014) and humans (Peyron et al., 2000; Thannickal et al., 2000). Consistent with this, we found a dramatic decrease in the firing rate of orexin neurons in Cx43 cKO^{GFAP} mice, which could result in a reduced release of orexin (Kiyashchenko et al., 2002). This correlation between reduced electrical activity of orexin neurons and decreased wakefulness is supported by in vivo studies showing that firing frequency of orexin neurons varies according to the vigilance state, increasing during wakefulness and diminishing during NREM sleep (Mileykovskiy et al., 2005; Lee et al., 2005; Adamantidis et al., 2007; Hassani et al., 2009; Tsunematsu et al., 2011).

In agreement with a previous study (Parsons and Hirasawa, 2010), we confirmed that spontaneous firing of orexin neurons primarily relies on the uptake of lactate through MCTs. Furthermore, we demonstrate that the effect of lactate was mediated through activation of LDH, which converts lactate to the metabolite pyruvate. We also found that lactate and pyruvate regulated firing and membrane potential of orexin neurons through the modulation of K_{ATP} channels, which have been shown to be expressed and functional in orexin neurons (Parsons and Hirasawa, 2010). Since LDH and K_{ATP} channels are well known to contribute to the metabolic regulation of neuronal excitation (Sada et al., 2015), our results allow us to confirm that orexin neurons preferentially use lactate rather than glucose as their source of energy to sustain neuronal activity.

In our study, we found that selective knockout of astroglial Cx43, which constitutes one of the molecular bases of astrocytic metabolic networks (Rouach et al., 2008), reduced dye-coupling between astrocytes in the LHA and perturbed the intercellular trafficking of glucose. As a consequence, orexin neurons had a decreased R_{in}, were hyperpolarized, and displayed a dramatic reduction in spontaneous firing rate, likely due to the opening of K_{ATP} channels caused by a lowering of intracellular ATP levels. Consistent with this idea, exogenous supply of the energy metabolite lactate depolarized the membrane and restored the activity of orexin neurons. This supports the ANLS hypothesis, in which lactate provided by astrocytes represents the major source of energy for neurons (Pellerin and Magistretti, 1994; Bélanger et al., 2011). While we identified a major role for MCTs in the metabolic effect of lactate on orexin neurons, this does not rule out the implication of Cx43 hemichannels in this effect, since they may also mediate basal release of lactate from astrocytes (Stehberg et al., 2012; Karagiannis et al., 2016).

We also found that bilateral injection of AAV-hGfa2-Cre:GFP in the LHA of Cx43$^{f/f}$ mice recapitulated the Cx43 cKO^{GFAP} phenotype of excessive sleepiness and fragmented wakefulness during the nocturnal active phase, suggesting that this phenotype was specific to the LHA. Consistent with our in vitro results, wakefulness stability was fully restored by delivery of lactate into the LHA, confirming that the sleep phenotype was caused by energy-deprived orexin neurons. Given the importance of astroglial Cx43 in various brain areas and functions such as memory, emotion, motor coordination, and sensory processing (Pannasch and Rouach, 2013; Oliveira et al., 2015), it is plausible that a deletion of astroglial Cx43 in another arousal nuclei may lead to a similar phenotype. This could be especially relevant in the locus coeruleus (LC), where astrocytic lactate acts on noradrenergic neurons as a signaling molecule to stimulate noradrenaline release (Tang et al., 2014).

Orexin neurons are strongly activated during the dark phase (Mileykovskiy et al., 2005; Lee et al., 2005; Hassani et al., 2009) and need a burst of fuel to heighten and maintain their tonic activity long enough to consolidate wakefulness. We show that the shuttling of energy metabolites through gap junction-mediated astrocytic networks is a prime candidate to efficiently provide this energy. Since each astrocyte can contact over 100,000 synapses (Bushong et al., 2002) and enwrap 4–8 neuronal somata (Halassa et al., 2007), the demand on one astrocyte for energy metabolite supply might be overwhelming. Thus, by increasing the effective volume of the intracellular compartment (De Pina-Benabou et al., 2001) and allowing glucose/lactate trafficking toward areas of high neuronal activity (Ball et al., 2007; Cruz et al., 2007; Rouach et al., 2008; Gandhi et al., 2009), gap junctional communication between astrocytes could provide better metabolic support to neurons than could be achieved by individual uncoupled astrocytes.

A role for gap junction-mediated astrocytic networks in the consolidation of wakefulness is further supported by the facts that astrocytic coupling changes depending on the vigilance state, increasing during wakefulness and decreasing during sleep (Petit and Magistretti, 2016), and that the wake-promoting drug modafinil, used to treat narcolepsy, can significantly increase gap junctional coupling between cortical astrocytes (Liu et al., 2013).

(E) Representative hypnograms of a control (left) and Cx43$^{f/f}$ mouse transduced with AAV (right). Bottom traces represent EEG/EMG recordings from ZT12 to ZT18.

(F and G) Average of the number (F) and duration (G) of wake, NREM, and REM sleep episodes during the 12 hr light and dark phases in control (n = 8) and Cx43$^{f/f}$ mice transduced with the AAV (n = 8; ANOVA followed by post hoc test; *p < 0.05, **p < 0.01, and ***p < 0.001).

(H) Average number of transitions between vigilance states (W, wake; N, NREM; R, REM) in control (n = 8) and Cx43$^{f/f}$ mice transduced with AAV (n = 8; ANOVA followed by post hoc test; *p < 0.05 and ***p < 0.01).

Pooled data are shown as mean ± SEM. See also Figure S5.

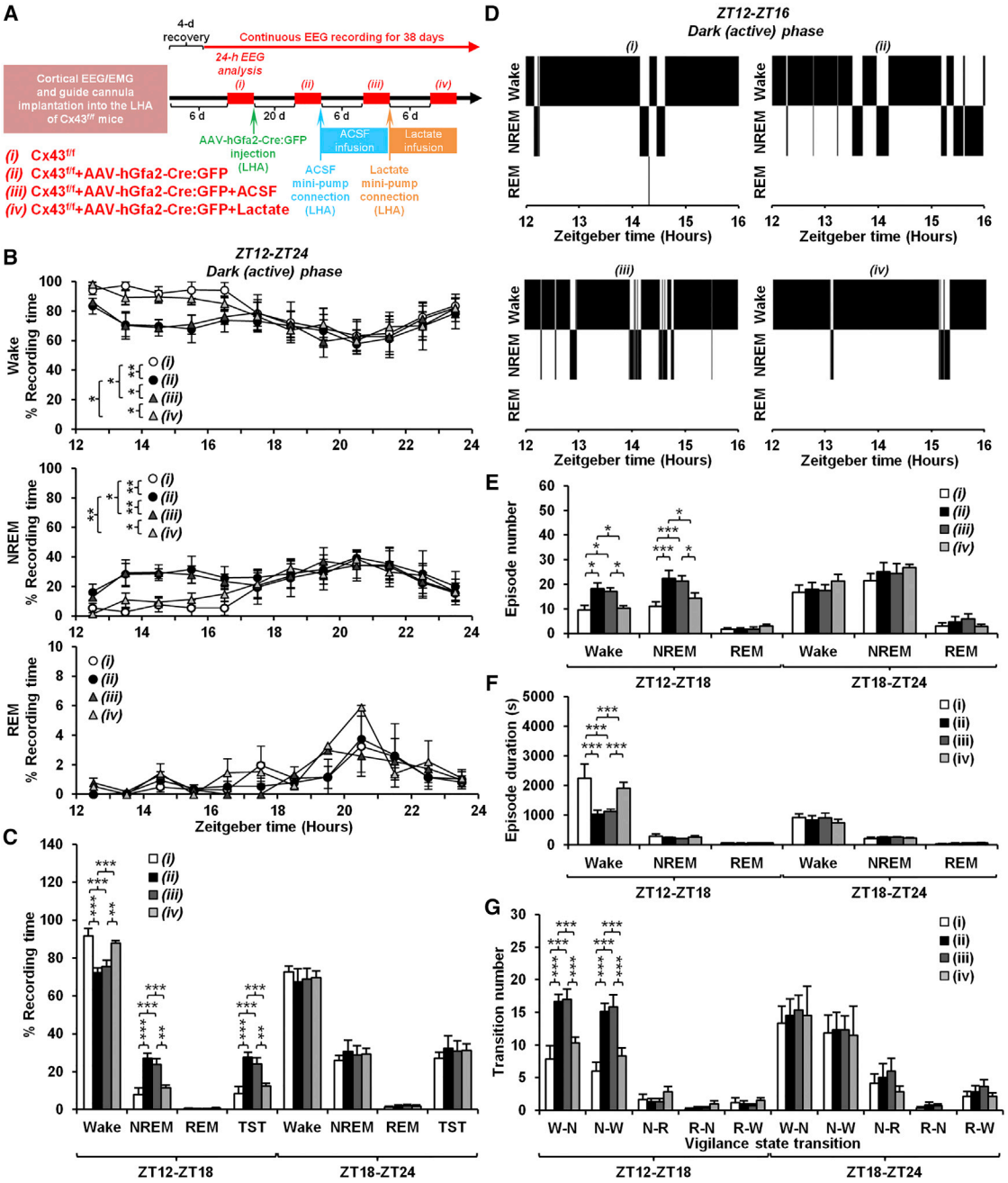

Figure 8. Lactate Abrogates Nocturnal Sleepiness and Instability of Wakefulness Induced by the Deletion of Cx43 in Astrocytes from the LHA

(A) Experimental design and timeline. Twenty-four-hour EEG recordings (ZT0–ZT24) were analyzed over time in the same Cx43$^{f/f}$ mouse (n = 6) at the four experimental time points (i, ii, iii, iv; red bars).

(B) Percentage average of the time spent in wake (top), NREM (middle), and REM sleep (bottom) per hour during the 12 hr dark phase at the four time points (ANOVA followed by post hoc test; *p < 0.05, **p < 0.01, and ***p < 0.001).

(C) Averaged percentage of time spent in wake, NREM, and REM sleep during the first (ZT12–ZT18) and last (ZT18–ZT24) 6 hr of the dark phase at the four time points (ANOVA followed by post hoc test; **p < 0.01 and ***p < 0.001). TST, total sleep time including REM and NREM sleep.

(D) Representative hypnograms of the same Cx43$^{f/f}$ mouse during the first 4 hr of the dark phase (ZT12–ZT16) at the four time points.

(E and F) Average of the number (E) and duration (F) of wake, NREM, and REM sleep episodes during the first (ZT12–ZT18) and last (ZT18–ZT24) 6 hr of the dark phase at the four time points (ANOVA followed by post hoc test; *p < 0.05 and ***p < 0.001).

(G) Average number of transitions between vigilance states (W, wake; N, NREM; R, REM) during the first (ZT12–ZT18) and last (ZT18–ZT24) 6 hr of the dark phase at the four time points (ANOVA followed by post hoc test; ***p < 0.001).

Pooled data are shown as mean ± SEM.

Recently, lactate has also been identified as biomarker for sleep-wake cycles (Naylor et al., 2012). High-resolution in vivo measurements of lactate in the brain via biosensors indicate that the analyte displays a daily variation with higher values during the active phase (Dash et al., 2013). Lactate also varies as a function of the sleep-wake cycle, increasing during wakefulness and decreasing during NREM sleep (Naylor et al., 2012; Dash et al., 2013; Wisor et al., 2013). Thus, our study provides direct evidence for the role of ANLS in wakefulness and remains in line with previous work showing that astrocyte-derived lactate is the preferred energy substrate for use by active neurons during awakening (Aubert et al., 2005; Wyss et al., 2011; Sampol et al., 2013; Bouzier-Sore and Pellerin, 2013; Magistretti and Allaman, 2015).

Excessive sleepiness and an inability to maintain sustained episodes of wakefulness during the active phase are characteristics of human (Scammell et al., 2009) and animal models of narcolepsy (Lin et al., 1999; Chemelli et al., 1999; Willie et al., 2003; Mochizuki et al., 2004; Tabuchi et al., 2014). The main cause of narcolepsy is a marked and selective loss of orexin neurons in the LHA (Peyron et al., 2000; Thannickal et al., 2000). Although the sleep-wake phenotype observed in Cx43 cKO^{GFAP} mice is reminiscent of a narcolepsy-like phenotype, our video-EEG recordings did not show any of the two main other features of narcolepsy: cataplectic attacks and sudden intrusions of REM sleep during awakening (Scammell et al., 2009). Furthermore, the number of orexin neurons in the LHA remained normal in Cx43 cKO^{GFAP} mice. Narcolepsy without cataplexy can be considered as an early form of narcolepsy during which the frequency of cataplectic attacks progressively increases subsequent to orexin neuron degeneration (Baumann et al., 2014; Tabuchi et al., 2014).

In conclusion, we propose a hitherto unknown regulatory mechanism of sleep-wake cycle involving astrocyte-neuron metabolic interactions. Using EEG, in vitro electrophysiology, and astrocytic-specific molecular genetics, we demonstrate that activity of orexin neurons depends on energy metabolites trafficking through astroglial metabolic networks, a mechanism that is critical for maintaining the normal daily cycle of wakefulness. We also provide strong evidence of the importance of ANLS in this process.

STAR★METHODS

Detailed methods are provided in the online version of this paper and include the following:

- KEY RESOURCES TABLE
- CONTACT FOR REAGENT AND RESOURCE SHARING
- EXPERIMENTAL MODEL AND SUBJECT DETAILS
  - Animals, housing, and genotyping
- METHOD DETAILS
  - Western blot analysis
  - EEG/EMG surgery, recording, and analysis
  - Adeno-associated virus vector
  - Stereotaxic virus injection
  - Virus and drug injections in freely behaving mice
  - Immunohistochemistry
  - Brain slice preparation
  - Patch-clamp recordings
  - Cell phenotyping and dye-coupling analysis
- QUANTIFICATION AND STATISTICAL ANALYSIS

SUPPLEMENTAL INFORMATION

Supplemental Information includes five figures and can be found with this article online at http://dx.doi.org/10.1016/j.neuron.2017.08.022.

AUTHOR CONTRIBUTIONS

J.C. and P.G.H. designed and supervised research. J.C. and E.S. performed research. J.C. analyzed data. Z.W. and D.B. contributed new reagents. J.C. and P.G.H. wrote the paper.

ACKNOWLEDGMENTS

P.G.H. was supported by NIH grants (R01 NS037585 and R01 AA020183); J.C. by the Epilepsy Foundation, Marie Skłodowska-Curie Actions—European Research Fellowship (H2020-MSCA-IF-2014, ID656657), and Région Hauts-de-France (program VisionAIRR); E.S. by NIH/NINDS (R01NS092466 and R01NS092786); and D.B. by the NINDS (R01 NS084920). P.G.H. has equity interest in GliaCure Inc.

Received: February 25, 2017
Revised: June 29, 2017
Accepted: August 14, 2017
Published: August 31, 2017

REFERENCES

Adamantidis, A.R., Zhang, F., Aravanis, A.M., Deisseroth, K., and de Lecea, L. (2007). Neural substrates of awakening probed with optogenetic control of hypocretin neurons. Nature *450*, 420–424.

Araque, A., Carmignoto, G., Haydon, P.G., Oliet, S.H., Robitaille, R., and Volterra, A. (2014). Gliotransmitters travel in time and space. Neuron *81*, 728–739.

Aubert, A., Costalat, R., Magistretti, P.J., and Pellerin, L. (2005). Brain lactate kinetics: Modeling evidence for neuronal lactate uptake upon activation. Proc. Natl. Acad. Sci. USA *102*, 16448–16453.

Ball, K.K., Gandhi, G.K., Thrash, J., Cruz, N.F., and Dienel, G.A. (2007). Astrocytic connexin distributions and rapid, extensive dye transfer via gap junctions in the inferior colliculus: implications for [(14)C]glucose metabolite trafficking. J. Neurosci. Res. *85*, 3267–3283.

Baumann, C.R., Mignot, E., Lammers, G.J., Overeem, S., Arnulf, I., Rye, D., Dauvilliers, Y., Honda, M., Owens, J.A., Plazzi, G., and Scammell, T.E. (2014). Challenges in diagnosing narcolepsy without cataplexy: a consensus statement. Sleep *37*, 1035–1042.

Bélanger, M., Allaman, I., and Magistretti, P.J. (2011). Brain energy metabolism: focus on astrocyte-neuron metabolic cooperation. Cell Metab. *14*, 724–738.

Bouzier-Sore, A.K., and Pellerin, L. (2013). Unraveling the complex metabolic nature of astrocytes. Front. Cell. Neurosci. *7*, 179.

Brand-Schieber, E., Werner, P., Iacobas, D.A., Iacobas, S., Beelitz, M., Lowery, S.L., Spray, D.C., and Scemes, E. (2005). Connexin43, the major gap junction protein of astrocytes, is down-regulated in inflamed white matter in an animal model of multiple sclerosis. J. Neurosci. Res. *80*, 798–808.

Brenner, M., Kisseberth, W.C., Su, Y., Besnard, F., and Messing, A. (1994). GFAP promoter directs astrocyte-specific expression in transgenic mice. J. Neurosci. *14*, 1030–1037.

Broekman, M.L., Comer, L.A., Hyman, B.T., and Sena-Esteves, M. (2006). Adeno-associated virus vectors serotyped with AAV8 capsid are more efficient

than AAV-1 or -2 serotypes for widespread gene delivery to the neonatal mouse brain. Neuroscience *138*, 501–510.

Brown, R.E., Basheer, R., McKenna, J.T., Strecker, R.E., and McCarley, R.W. (2012). Control of sleep and wakefulness. Physiol. Rev. *92*, 1087–1187.

Bushong, E.A., Martone, M.E., Jones, Y.Z., and Ellisman, M.H. (2002). Protoplasmic astrocytes in CA1 stratum radiatum occupy separate anatomical domains. J. Neurosci. *22*, 183–192.

Casper, K.B., and McCarthy, K.D. (2006). GFAP-positive progenitor cells produce neurons and oligodendrocytes throughout the CNS. Mol. Cell. Neurosci. *31*, 676–684.

Chemelli, R.M., Willie, J.T., Sinton, C.M., Elmquist, J.K., Scammell, T., Lee, C., Richardson, J.A., Williams, S.C., Xiong, Y., Kisanuki, Y., et al. (1999). Narcolepsy in orexin knockout mice: molecular genetics of sleep regulation. Cell *98*, 437–451.

Clasadonte, J., Dong, J., Hines, D.J., and Haydon, P.G. (2013). Astrocyte control of synaptic NMDA receptors contributes to the progressive development of temporal lobe epilepsy. Proc. Natl. Acad. Sci. USA *110*, 17540–17545.

Clasadonte, J., McIver, S.R., Schmitt, L.I., Halassa, M.M., and Haydon, P.G. (2014). Chronic sleep restriction disrupts sleep homeostasis and behavioral sensitivity to alcohol by reducing the extracellular accumulation of adenosine. J. Neurosci. *34*, 1879–1891.

Cruz, N.F., Ball, K.K., and Dienel, G.A. (2007). Functional imaging of focal brain activation in conscious rats: impact of [(14)C]glucose metabolite spreading and release. J. Neurosci. Res. *85*, 3254–3266.

Dash, M.B., Bellesi, M., Tononi, G., and Cirelli, C. (2013). Sleep/wake dependent changes in cortical glucose concentrations. J. Neurochem. *124*, 79–89.

De Pina-Benabou, M.H., Srinivas, M., Spray, D.C., and Scemes, E. (2001). Calmodulin kinase pathway mediates the K^+-induced increase in Gap junctional communication between mouse spinal cord astrocytes. J. Neurosci. *21*, 6635–6643.

Eggermann, E., Bayer, L., Serafin, M., Saint-Mleux, B., Bernheim, L., Machard, D., Jones, B.E., and Mühlethaler, M. (2003). The wake-promoting hypocretin-orexin neurons are in an intrinsic state of membrane depolarization. J. Neurosci. *23*, 1557–1562.

Gandhi, G.K., Cruz, N.F., Ball, K.K., and Dienel, G.A. (2009). Astrocytes are poised for lactate trafficking and release from activated brain and for supply of glucose to neurons. J. Neurochem. *111*, 522–536.

Giaume, C., and Theis, M. (2010). Pharmacological and genetic approaches to study connexin-mediated channels in glial cells of the central nervous system. Brain Res. Brain Res. Rev. *63*, 160–176.

Giaume, C., Koulakoff, A., Roux, L., Holcman, D., and Rouach, N. (2010). Astroglial networks: a step further in neuroglial and gliovascular interactions. Nat. Rev. Neurosci. *11*, 87–99.

Goodenough, D.A., Goliger, J.A., and Paul, D.L. (1996). Connexins, connexons, and intercellular communication. Annu. Rev. Biochem. *65*, 475–502.

Halassa, M.M., Fellin, T., Takano, H., Dong, J.H., and Haydon, P.G. (2007). Synaptic islands defined by the territory of a single astrocyte. J. Neurosci. *27*, 6473–6477.

Halassa, M.M., Florian, C., Fellin, T., Munoz, J.R., Lee, S.Y., Abel, T., Haydon, P.G., and Frank, M.G. (2009). Astrocytic modulation of sleep homeostasis and cognitive consequences of sleep loss. Neuron *61*, 213–219.

Halestrap, A.P., and Price, N.T. (1999). The proton-linked monocarboxylate transporter (MCT) family: structure, function and regulation. Biochem. J. *343*, 281–299.

Han, Y., Yu, H.X., Sun, M.L., Wang, Y., Xi, W., and Yu, Y.Q. (2014). Astrocyte-restricted disruption of connexin-43 impairs neuronal plasticity in mouse barrel cortex. Eur. J. Neurosci. *39*, 35–45.

Hassani, O.K., Lee, M.G., and Jones, B.E. (2009). Melanin-concentrating hormone neurons discharge in a reciprocal manner to orexin neurons across the sleep-wake cycle. Proc. Natl. Acad. Sci. USA *106*, 2418–2422.

Karagiannis, A., Sylantyev, S., Hadjihambi, A., Hosford, P.S., Kasparov, S., and Gourine, A.V. (2016). Hemichannel-mediated release of lactate. J. Cereb. Blood Flow Metab. *36*, 1202–1211.

Kiyashchenko, L.I., Mileykovskiy, B.Y., Maidment, N., Lam, H.A., Wu, M.F., John, J., Peever, J., and Siegel, J.M. (2002). Release of hypocretin (orexin) during waking and sleep states. J. Neurosci. *22*, 5282–5286.

Lam, T.K., Gutierrez-Juarez, R., Pocai, A., and Rossetti, L. (2005). Regulation of blood glucose by hypothalamic pyruvate metabolism. Science *309*, 943–947.

Lee, M.G., Hassani, O.K., and Jones, B.E. (2005). Discharge of identified orexin/hypocretin neurons across the sleep-waking cycle. J. Neurosci. *25*, 6716–6720.

Lee, Y., Messing, A., Su, M., and Brenner, M. (2008). GFAP promoter elements required for region-specific and astrocyte-specific expression. Glia *56*, 481–493.

Liao, Y., Day, K.H., Damon, D.N., and Duling, B.R. (2001). Endothelial cell-specific knockout of connexin 43 causes hypotension and bradycardia in mice. Proc. Natl. Acad. Sci. USA *98*, 9989–9994.

Lin, L., Faraco, J., Li, R., Kadotani, H., Rogers, W., Lin, X., Qiu, X., de Jong, P.J., Nishino, S., and Mignot, E. (1999). The sleep disorder canine narcolepsy is caused by a mutation in the hypocretin (orexin) receptor 2 gene. Cell *98*, 365–376.

Liu, X., Petit, J.M., Ezan, P., Gyger, J., Magistretti, P., and Giaume, C. (2013). The psychostimulant modafinil enhances gap junctional communication in cortical astrocytes. Neuropharmacology *75*, 533–538.

Magistretti, P.J., and Allaman, I. (2015). A cellular perspective on brain energy metabolism and functional imaging. Neuron *86*, 883–901.

Martin, K.R., Klein, R.L., and Quigley, H.A. (2002). Gene delivery to the eye using adeno-associated viral vectors. Methods *28*, 267–275.

Matsuda, T., and Cepko, C.L. (2007). Controlled expression of transgenes introduced by in vivo electroporation. Proc. Natl. Acad. Sci. USA *104*, 1027–1032.

Mileykovskiy, B.Y., Kiyashchenko, L.I., and Siegel, J.M. (2005). Behavioral correlates of activity in identified hypocretin/orexin neurons. Neuron *46*, 787–798.

Mochizuki, T., Crocker, A., McCormack, S., Yanagisawa, M., Sakurai, T., and Scammell, T.E. (2004). Behavioral state instability in orexin knock-out mice. J. Neurosci. *24*, 6291–6300.

Nagy, J.I., and Rash, J.E. (2000). Connexins and gap junctions of astrocytes and oligodendrocytes in the CNS. Brain Res. Brain Res. Rev. *32*, 29–44.

Naylor, E., Aillon, D.V., Barrett, B.S., Wilson, G.S., Johnson, D.A., Johnson, D.A., Harmon, H.P., Gabbert, S., and Petillo, P.A. (2012). Lactate as a biomarker for sleep. Sleep *35*, 1209–1222.

Oliveira, J.F., Sardinha, V.M., Guerra-Gomes, S., Araque, A., and Sousa, N. (2015). Do stars govern our actions? Astrocyte involvement in rodent behavior. Trends Neurosci. *38*, 535–549.

Pannasch, U., and Rouach, N. (2013). Emerging role for astroglial networks in information processing: from synapse to behavior. Trends Neurosci. *36*, 405–417.

Parsons, M.P., and Hirasawa, M. (2010). ATP-sensitive potassium channel-mediated lactate effect on orexin neurons: implications for brain energetics during arousal. J. Neurosci. *30*, 8061–8070.

Paukert, M., Agarwal, A., Cha, J., Doze, V.A., Kang, J.U., and Bergles, D.E. (2014). Norepinephrine controls astroglial responsiveness to local circuit activity. Neuron *82*, 1263–1270.

Pellerin, L., and Magistretti, P.J. (1994). Glutamate uptake into astrocytes stimulates aerobic glycolysis: a mechanism coupling neuronal activity to glucose utilization. Proc. Natl. Acad. Sci. USA *91*, 10625–10629.

Petit, J.M., and Magistretti, P.J. (2016). Regulation of neuron-astrocyte metabolic coupling across the sleep-wake cycle. Neuroscience *323*, 135–156.

Peyron, C., Faraco, J., Rogers, W., Ripley, B., Overeem, S., Charnay, Y., Nevsimalova, S., Aldrich, M., Reynolds, D., Albin, R., et al. (2000). A mutation

in a case of early onset narcolepsy and a generalized absence of hypocretin peptides in human narcoleptic brains. Nat. Med. *6*, 991–997.

Rouach, N., Koulakoff, A., Abudara, V., Willecke, K., and Giaume, C. (2008). Astroglial metabolic networks sustain hippocampal synaptic transmission. Science *322*, 1551–1555.

Sada, N., Lee, S., Katsu, T., Otsuki, T., and Inoue, T. (2015). Epilepsy treatment. Targeting LDH enzymes with a stiripentol analog to treat epilepsy. Science *347*, 1362–1367.

Sakurai, T. (2007). The neural circuit of orexin (hypocretin): maintaining sleep and wakefulness. Nat. Rev. Neurosci. *8*, 171–181.

Sampol, D., Ostrofet, E., Jobin, M.L., Raffard, G., Sanchez, S., Bouchaud, V., Franconi, J.M., Bonvento, G., and Bouzier-Sore, A.K. (2013). Glucose and lactate metabolism in the awake and stimulated rat: a (13)C-NMR study. Front. Neuroenergetics *5*, 5.

Scammell, T.E., Willie, J.T., Guilleminault, C., and Siegel, J.M.; International Working Group on Rodent Models of Narcolepsy (2009). A consensus definition of cataplexy in mouse models of narcolepsy. Sleep *32*, 111–116.

Schindelin, J., Arganda-Carreras, I., Frise, E., Kaynig, V., Longair, M., Pietzsch, T., Preibisch, S., Rueden, C., Saalfeld, S., Schmid, B., et al. (2012). Fiji: an open-source platform for biological-image analysis. Nat. Methods *9*, 676–682.

Sontheimer, H. (1994). Voltage-dependent ion channels in glial cells. Glia *11*, 156–172.

Stehberg, J., Moraga-Amaro, R., Salazar, C., Becerra, A., Echeverría, C., Orellana, J.A., Bultynck, G., Ponsaerts, R., Leybaert, L., Simon, F., et al. (2012). Release of gliotransmitters through astroglial connexin 43 hemichannels is necessary for fear memory consolidation in the basolateral amygdala. FASEB J. *26*, 3649–3657.

Steinhäuser, C. (1993). Electrophysiologic characteristics of glial cells. Hippocampus *3*, 113–123.

Tabuchi, S., Tsunematsu, T., Black, S.W., Tominaga, M., Maruyama, M., Takagi, K., Minokoshi, Y., Sakurai, T., Kilduff, T.S., and Yamanaka, A. (2014). Conditional ablation of orexin/hypocretin neurons: a new mouse model for the study of narcolepsy and orexin system function. J. Neurosci. *34*, 6495–6509.

Tang, F., Lane, S., Korsak, A., Paton, J.F., Gourine, A.V., Kasparov, S., and Teschemacher, A.G. (2014). Lactate-mediated glia-neuronal signalling in the mammalian brain. Nat. Commun. *5*, 3284.

Thannickal, T.C., Moore, R.Y., Nienhuis, R., Ramanathan, L., Gulyani, S., Aldrich, M., Cornford, M., and Siegel, J.M. (2000). Reduced number of hypocretin neurons in human narcolepsy. Neuron *27*, 469–474.

Theis, M., Jauch, R., Zhuo, L., Speidel, D., Wallraff, A., Döring, B., Frisch, C., Söhl, G., Teubner, B., Euwens, C., et al. (2003). Accelerated hippocampal spreading depression and enhanced locomotory activity in mice with astrocyte-directed inactivation of connexin43. J. Neurosci. *23*, 766–776.

Tsunematsu, T., Kilduff, T.S., Boyden, E.S., Takahashi, S., Tominaga, M., and Yamanaka, A. (2011). Acute optogenetic silencing of orexin/hypocretin neurons induces slow-wave sleep in mice. J. Neurosci. *31*, 10529–10539.

Wiencken-Barger, A.E., Djukic, B., Casper, K.B., and McCarthy, K.D. (2007). A role for Connexin43 during neurodevelopment. Glia *55*, 675–686.

Willie, J.T., Chemelli, R.M., Sinton, C.M., Tokita, S., Williams, S.C., Kisanuki, Y.Y., Marcus, J.N., Lee, C., Elmquist, J.K., Kohlmeier, K.A., et al. (2003). Distinct narcolepsy syndromes in Orexin receptor-2 and Orexin null mice: molecular genetic dissection of Non-REM and REM sleep regulatory processes. Neuron *38*, 715–730.

Wisor, J.P., Rempe, M.J., Schmidt, M.A., Moore, M.E., and Clegern, W.C. (2013). Sleep slow-wave activity regulates cerebral glycolytic metabolism. Cereb. Cortex *23*, 1978–1987.

Wyss, M.T., Jolivet, R., Buck, A., Magistretti, P.J., and Weber, B. (2011). In vivo evidence for lactate as a neuronal energy source. J. Neurosci. *31*, 7477–7485.

Zolotukhin, S., Byrne, B.J., Mason, E., Zolotukhin, I., Potter, M., Chesnut, K., Summerford, C., Samulski, R.J., and Muzyczka, N. (1999). Recombinant adeno-associated virus purification using novel methods improves infectious titer and yield. Gene Ther. *6*, 973–985.

STAR★METHODS

KEY RESOURCES TABLE

REAGENT or RESOURCE	SOURCE	IDENTIFIER
Antibodies		
Chicken polyclonal anti-GFAP	Abcam	Cat#ab4674; RRID: AB_304558
Rabbit polyclonal anti-orexin-A	Millipore	Cat#AB3704 RRID: AB_91545
Mouse monoclonal anti-NeuN	Millipore	Cat#MAB377; RRID: AB_2298772
Rabbit polyclonal anti-Cx43	Sigma	Cat#C6219; RRID: AB_476857
Mouse monoclonal anti-GAPDH	Fitzgerald	Cat#10R-G109a; RRID: AB_1285808
HRP-conjugated goat polyclonal anti-rabbit	Santa Cruz Biotechnology	Cat#sc-2004; RRID: AB_631746
HRP-conjugated goat polyclonal anti-mouse	Santa Cruz Biotechnology	Cat#sc-2005; RRID: AB_631736
Goat polyclonal anti-chicken, Alexa Fluor 633 conjugate	Invitrogen	Cat#A-21103; RRID: AB_2535756
Goat polyclonal anti-rabbit, Alexa Fluor 546 conjugate	Invitrogen	Cat#A-11035; RRID: AB_2534093
Goat polyclonal anti-rabbit, Alexa Fluor 488 conjugate	Invitrogen	Cat#A-11034; RRID: AB_2576217
Goat polyclonal anti-mouse, Alexa Fluor 546 conjugate	Invitrogen	Cat#A-11030; RRID: AB_2534089
Bacterial and Virus Strains		
AAV8-hGfa2-Cre:GFP	This paper	N/A
Chemicals, Peptides, and Recombinant Proteins		
Sodium L-lactate	Alfa Aesar	Cat#L14500; CAS: 867-56-1
Sodium pyruvate	Sigma	Cat#P8574; CAS: 113-24-6
Sodium oxamate	Sigma	Cat#O2751; CAS: 565-73-1
Tolbutamide	Sigma	Cat#T0891; CAS: 64-77-7
TTX (Tetrodotoxin citrate)	Tocris	Cat#1069; CAS: 18660-81-6
4-CIN (Alpha-cyano-4-hydroxycinnamic acid)	Sigma	Cat#C2020; CAS: 28166-41-8
Carbenoxolone disodium salt	Sigma	Cat#C4790; CAS:7424-40-1
Biocytin	Sigma	Cat#B-4261; CAS: 576-19-2
2-NBDG (2-[N-(7-nitrobenz-2-oxa-1,3-diazol-4-yl) amino]-2-deoxyglucose)	Invitrogen	Cat#N13195; CAS: 186689-07-6
Dextran tetramethylrhodamine	Invitrogen	Cat#D1868
Alexa Fluor 594 hydrazide	Invitrogen	Cat#A10438
Lucifer yellow CH dilithium salt	Sigma	Cat#L0259; CAS: 67769-47-5
Streptavidin, Alexa Fluor 546 conjugate	Invitrogen	Cat#S11225
Streptavidin, Alexa Fluor 488 conjugate	Invitrogen	Cat#S11223; CAS: 366796-16-9
Experimental Models: Organisms/Strains		
Mouse: Cx43$^{f/f}$ (B6.129S7-*Gja1*^{tm1Dlg}/J)	Liao et al., 2001; The Jackson Laboratory	Jax No.: 008039
Mouse: hGFAP-Cre	Casper and McCarthy, 2006	N/A
Mouse: Cx43 cKO^{GFAP} (Cx43$^{f/f}$:hGFAP-Cre+)	This paper; Wiencken-Barger et al., 2007	N/A
Oligonucleotides		
Primer Cx43$^{f/f}$ Forward: CTTTGACTCTGATTACA GAGCTTAA	This paper	N/A
Primer Cx43$^{f/f}$ Reverse: GTCTCACTGTTACTTAAC AGCTTGA	This paper	N/A
Primer hGFAP-Cre Forward: GGTCGATGCAAC GAGTGATGAGG	This paper	N/A
Primer hGFAP-Cre Reverse: GCTAAGTGCCTTCTC TACACCTGCG	This paper	N/A

(*Continued on next page*)

Continued

REAGENT or RESOURCE	SOURCE	IDENTIFIER
Software and Algorithms		
SleepSign for Animals	Kissei Comtec	http://www.sleepsign.com/
Sirenia	Pinnacle Technology	https://www.pinnaclet.com/software.html
Fiji	Schindelin et al., 2012	https://fiji.sc/
pClamp 9.2	Molecular Devices	http://mdc.custhelp.com/app/answers/detail/a_id/18826/related/1
pClamp 10.6	Molecular Devices	http://mdc.custhelp.com/app/answers/detail/a_id/18779
SigmaPlot 11 and 13	Systat	https://systatsoftware.com/
Other		
Synchonized video-EEG/EMG system	Pinnacle Technology	https://www.pinnaclet.com/eeg-emg-systems.html

CONTACT FOR REAGENT AND RESOURCE SHARING

Further information and requests for resources and reagents should be directed to and will be fulfilled by the Lead Contact, Philip Haydon (philip.haydon@tufts.edu).

EXPERIMENTAL MODEL AND SUBJECT DETAILS

Animals, housing, and genotyping

Astrocyte-specific Cx43 conditional knockout (cKO) mice were generated with the Cre/LoxP system by breeding homozygous floxed Cx43 mice ($Cx43^{f/f}$; Liao et al., 2001) to human glial fibrillary acidic protein (hGFAP)-Cre mice (Casper and McCarthy, 2006), as previously reported (Wiencken-Barger et al., 2007; Han et al., 2014). $Cx43^{f/f}$ and hGFAP-Cre transgenic lines were obtained from Dr. Ken D. McCarthy (Department of Pharmacology, University of North Carolina, Chapel Hill, NC, USA). In $Cx43^{f/f}$ mice, Exon 2 of Cx43 allele was flanked by two LoxP sites, while in GFAP-Cre mice, a DNA fragment encoding Cre recombinase was inserted into an expression cassette containing a 2.2 kb human GFAP promoter, *gfa2*, to drive the expression of inducible Cre recombinase in GFAP-expressing cells. Homozygous floxed Cx43 mice and hGFAP-Cre mice were backcrossed for at least 10 generations to C57BL/6J mice before intercrossing. To generate experimental animals, homozygous floxed Cx43 Cre-positive mice ($Cx43^{f/f}$:hGFAP-Cre+ aka Cx43 cKO^{GFAP}) were bred to homozygous floxed Cre-negative mice ($Cx43^{f/f}$:hGFAP-Cre- aka $Cx43^{f/f}$). The resulting offspring were all homozygous floxed and either hemizygous or negative for hGFAP-Cre. The following primers were used for PCR genotyping from tail DNA: for floxed Cx43 (WT band 400 bp; floxed band 450 bp) forward 5′-CTTTGACTCTGATTACAGAGCTTAA-3′ and reverse 5′- GTCTCACTGTTACTTAACAGCTTGA-3′; for hGFAP-Cre (500 bp band) forward 5′-GGTCGATGCAACGAGTGATGAGG-3′ and reverse 5′-GCTAAGTGCCTTCTCTACACCTGCG-3′. Littermates with homozygous floxed Cre-negative ($Cx43^{f/f}$) or WT mice with the same C57BL/6J genetic background were used as controls as specified in the results.

Mice were bred and housed on a 12/12 light/dark cycle (8 am/8 pm) and given standard chow and water ad libitum. These experiments were performed with the approval of the Institutional Animal Care and Use Committee of Tufts University and the Universities of Lille, and under the guidelines defined by the National Institutes of Health Guide for the Care and Use of Laboratory Animals and the the European Union Council Directive of September 22, 2010 (2010/63/EU).

METHOD DETAILS

Western blot analysis

Eight weeks old male mice were anesthetized with isoflurane prior to decapitation. Brains were rapidly removed from the skull and frozen at −80°C until processed for protein extractions. Homogenates from whole-brain tissues were prepared as previously described (Brand-Schieber et al., 2005). Frozen brains were placed in lysis buffer (50 mM NaCl, 25 mM Tris–HCl, 5 mM EDTA, 1% NP-40, 0.25 mM Na-deoxycholate, pH 7.5) and tissue sonicated. Samples of whole-cell lysates in Laemmli buffer (20 μg total protein) were electrophoresed in 4%–20% SDS-PAGE (Bio-Rad, Hercules, CA) and then transferred to nitrocellulose membranes (Schleicher & Schuell, Keene, NH, USA). Immunoblots were performed after overnight incubation of membranes with blocking solution (5% dry nonfat milk and 0.4% polyoxyethylenesorbitan monolaurate: Tween-20; Sigma) using the following primary antibodies: rabbit polyclonal anti-connexin43 (1:2000, Sigma) and mouse monoclonal anti-GAPDH (1:5000, Fitzgerald).

After several washes with 1X PBS-Tween-20, membranes were incubated with the following HRP-conjugated secondary antibodies: goat polyclonal anti-rabbit (1:2000, Santa Cruz Biotechnology, Santa Cruz, CA, USA) and goat polyclonal anti-mouse

(1:2000, Santa Cruz Biotechnology, Santa Cruz, CA, USA). Detection of bands was performed on X-ray films (Kodak, Rochester, NY, USA) following incubation with enhanced chemiluminescence reagents (Amersham Pharmacia Biotechnology, Piscataway, NJ, USA).

EEG/EMG surgery, recording, and analysis

Electroencephalogram (EEG)/electromyogram (EMG) implantation surgery was performed as previously described (Clasadonte et al., 2013; 2014). Eight weeks old male $Cx43^{f/f}$, $Cx43\ cKO^{GFAP}$ and WT mice were anaesthetized with isoflurane and placed into a stereotaxic frame. For implantation of EEG electrodes, skull surface was exposed, and four insulated wire electrodes (Cooner Wire) were placed and screwed as follows: two extradural cortical electrodes were inserted bilaterally in the frontal areas and the two others were inserted bilaterally in the parietal areas. For implantation of EMG, two insulated wire electrodes were inserted bilaterally into the nuchal muscle. Electrodes connected to a microconnector (Pinnacle Technology) were secured at the surface of the skull with dental acrylic. After surgery, mice were intraperitoneally injected with buprenorphine (0.08 mg/kg) and lactated Ringer solution, fed with soaked rodent food. After 4 days of post-operative recovery, freely moving mice were placed into individual topless Plexiglas circle boxes (Pinnacle Technology) containing water and food ad libitum and their microconnectors plugged to a lightweight EEG preamplifier (Pinnacle Technology). Animals were acclimated for two days before data collection, monitored with video camera system (Pinnacle Technology) and maintained on a 8 am/8 pm light/dark cycle.

EEG and EMG signals were band-pass filtered at 1-100 Hz, digitized at 200 Hz, and acquired with a computer-based system and Sirenia software (Pinnacle Technology). Sleep stages were scored visually based on 4 s epochs by a trained experimenter using SleepSign for Animal software (Kissei Comtec). Wakefulness (W) consisted of low-amplitude, high-frequency EEG and high EMG activity; rapid eye movement (REM) sleep consisted of low-amplitude, desynchronized EEG with low EMG activity; and non-rapid eye movement (NREM) sleep consisted of high-amplitude, low-frequency EEG with little EMG modulation. Brief awakenings defined as uninterrupted waking episodes of 1-4 s epochs were not included in the analysis. Epochs containing movement artifacts were included in the state totals. After assignments of state scores, the amount of each state (expressed as a percentage of the total recording time in 1 hr time bins) and their duration were measured.

Adeno-associated virus vector

To selectively delete Cx43 from LHA astrocytes in $Cx43^{f/f}$ mice, we produced a recombinant AAV expression plasmid by placing a Cre:GFP fusion protein (Addgene, Cambridge, MA; Matsuda and Cepko, 2007) under control of the astrocyte-specific human GFAP promoter, hGfa2 (Addgene, Cambridge, MA; Brenner et al., 1994; Lee et al., 2008). AAV constructs also contained a 3′ woodchuck hepatitis virus posttranscriptional regulatory element (WPRE) to induce expression of intronless viral messages and increase the stability and level of gene expression (Martin et al., 2002). Recombinant AAV8 was packaged in cultures of HEK293T cells. Approximately 1.5×10^7 293T cells were seeded into 150 cm dishes in complete DMEM supplemented with 10% fetal bovine serum, 1 mM MEM sodium pyruvate, 0.1 mM MEM nonessential amino acids solution, and 0.05% Penicillin-Streptomycin (5,000 units/mL). At 24 hr media was changed to culture media containing 5% FBS and cells were transfected three separate plasmids: 1) Adeno helper plasmid (pFΔ6), 2) AAV helper encoding the Rep 2 and Cap 8 sequences for serotype 8 (pAR8; Broekman et al., 2006), and 3) the recombinant Cre:GFP expression plasmid described above. After culturing cells for 48 hr at 37°C, 5% CO_2, cells were harvested and pelleted by centrifugation. The pellet was resuspended in 10 mM Tris, pH 8.0 and chilled on ice. Cells were lysed by repeated freeze-thaw cycles followed by treatment with 50 U benzonase (Novagen, CA) and 0.5% sodium deoxycholate for 30 min at 37°C. Virus was purified by density gradient centrifugation in iodixinol (Zolotukhin et al., 1999). Two buffer exchanges with ACSF were performed. The purified virus was then concentrated in ACSF by centrifugation in Amicon Ultra-15 Centrifugal Filter Units. The final preparation was sterile filtered through a milipore syringe filter. The titer of each virus (2.1×10^{12} virus genomes per mL) was determined by quantitative RT-PCR using primers and a probe specific for the WPRE sequence.

Stereotaxic virus injection

Eight weeks old male $Cx43^{f/f}$ mice were anesthetized with isoflurane, placed into a stereotaxic frame and two small holes were bilaterally opened in the skull. A 2 μL Neuro 7002 syringe (Hamilton) was filled with AAV (1×10^9 virus genomes per μL) and the needle inserted into the lateral hypothalamic area (LHA; coordinate AP/DV/ML = −1.6/-5.35/ ± 0.9 mm). One μL of vector per hemisphere was injected with pressure at a speed of 0.10 μL/min using a Microsyringe Pump Controller Micro4 (World Precision Instruments). For controls, AAV and artificial cerebrospinal fluid (ACSF) were injected into the LHA of WT and $Cx43^{f/f}$ mice, respectively. Mice were allowed to recover for 10 days before the implantation of EEG/EMG electrodes, as described earlier.

Virus and drug injections in freely behaving mice

Eight week old male $Cx43^{f/f}$ mice were anesthetized with isoflurane, placed into a stereotaxic frame and two small holes were bilaterally opened in the skull. Bilateral brain cannula was stereotaxically implanted into the LHA (coordinate AP/DV/ML = −1.6/-5.35/ ± 0.9 mm). Mice were then implanted with EEG/EMG electrodes, as described earlier. After 4 days of post-operative recovery, freely moving mice were placed into individual topless Plexiglas circle boxes and their microconnectors plugged to

EEG preamplifier, as described earlier. One week after surgery, 1 μL of vector per hemisphere was injected into the LHA of freely behaving mice through the bilateral cannula with pressure at a speed of 0.10 μL/min using a Microsyringe Pump Controller Micro4 (World Precision Instruments).

Osmotic mini-pumps (model 1002; Alzet; flow rate, 0.25 μL/h; 2-wk duration) were filled with sodium L-lactate (5 mM in ACSF; Alfa Aesar) or vehicle (ACSF for control injection), secured with the flow moderator, and primed overnight in 0.9% saline solution at 37°C before to be connected to the brain cannula by flexible catheter tubing. Osmotic mini-pumps were externalized as previously described (Clasadonte et al., 2013). Briefly, they were placed in a sealed conic tube of 1 mL filled with 0.9% saline solution, and maintained at 37°C with a iBlock Mini Dry Bath (Midsci) placed out of the cage. The catheter tubing was filled with lactate (5 mM in ACSF; Alfa Aesar) or vehicle (ACSF for control injection). A small air bubble was inserted into the catheter tubing during its connection with the pump to monitor the flow rate estimated at 0.25 μL/h in our conditions. The flexible catheter tubing was carefully aligned and attached to the EEG cable. The presence of a swivel (Pinnacle Technology) prevented the torsion of tubing and cable. ACSF control injection was performed 21 days after the virus injection. One week later, catheter tubing and mini-pumps filled with ACSF and connected to the bilateral cannula were removed and replaced with catheter tubing and mini-pumps filled with sodium L-lactate (5 mM in ACSF; Alfa Aesar). Lactate infusion lasted for one week.

Immunohistochemistry

To map the AAV-hGfa2-Cre:GFP injection sites and cell targeting specificity, brain sections were immunostained after completion of the experiments. Mice were deeply anesthetized with a mixture of ketamine hydrochloride and xylazine hydrochloride. They were perfused sequentially via the left ventricle with 20 mL chilled phosphate buffer saline (PBS) solution (1x) and 100 mL 4% paraformaldehyde in PBS solution (1x, pH 7.4). Brains were removed and postfixed in the same fixative for 24 hr at 4°C. After fixation, they were soaked 24 hr in a solution of 30% sucrose. Coronal sections containing the LHA were cut serially at 200-μm intervals on a freezing microtome (SM2000R; Leica) at a thickness of 40 μm and then stored in an antifreeze solution at −20°C until immunostaining. For determining cell targeting specificity of AAV, double-immunostaining GFAP/orexin-A or GFAP/neuronal nuclei (NeuN) was conducted on free-floating sections incubated with 5% normal goat serum (NGS) blocking solution for 1 hr at room temperature and then with primary antibodies overnight at 4°C on a shaking platform. The chicken anti-GFAP antibody (1:1000; Abcam) was combined with either the rabbit anti-orexin-A antibody (1:1000; Millipore) or the mouse anti-NeuN antibody (1:1000; Millipore). Sections were rinsed three times with 1x PBS solution and then incubated with secondary antibodies for 2 hr at room temperature. The following secondary antibodies were used: goat anti-chicken Alexa Fluor 633 (1:1000; Invitrogen) with goat anti-rabbit Alexa Fluor 546 (1:1000; Invitrogen) or goat anti-chicken Alexa Fluor 633 (1:1000; Invitrogen) with goat anti-mouse Alexa Fluor 546 (1:1000; Invitrogen). All sections were counterstained with DAPI, mounted on slides and coverslipped with Vectashield antifade mounting medium. Due to GFP expression, the site of AAV injection was clearly observable using an epifluorescence microscope (Keyence BZ-X700). Entire sections were automatically imaged with a 10x objective and stitched with Keyence software. To examine cell targeting specificity, fluorescent images were acquired with a confocal laser scanning microscope (Nikon A1) using a 40x objective. Image analysis and counting of cells expressing GFP alone, GFP with GFAP, GFP with orexin-A and GFP with NeuN were performed within an area of interest in the LHA by using Fiji software.

To determine the number of orexin neurons in $Cx43^{f/f}$ and $Cx43\ cKO^{GFAP}$ mice that were not transduced with AAV, the same immunohistochemical procedure as stated above was followed by using the rabbit anti-orexin-A primary antibody (1:1000; Millipore) and the goat anti-rabbit Alexa Fluor 546 secondary antibody (1:1000; Invitrogen). Fluorescent images were acquired with a confocal laser scanning microscope (Nikon A1) using a 20x objective. Orexin-A-immunopositive cells were bilaterally counted in a square region (634.88 μm x 634.88 μm) within the LHA in all the sections that had fluorescent cell bodies by using Fiji software.

Brain slice preparation

Eight weeks old male $Cx43^{f/f}$ and $Cx43\ cKO^{GFAP}$ mice were anaesthetized with isoflurane, and after decapitation, the brain was rapidly removed and put in ice-cold oxygenated (O_2 95% / CO_2 5%) artificial cerebrospinal fluid (ACSF) containing the following (in mM): 120 NaCl, 3.2 KCl, 1 NaH_2PO_4, 26 $NaHCO_3$, 1 $MgCl_2$, 2 $CaCl_2$, 2.5 glucose (osmolarity adjusted to 300 mOsm with sucrose, pH 7.4). After removal of the cerebellum, the brain was glued and coronal hypothalamic slices containing the LHA were cut using a vibratome (VT1200S; Leica). Before recording, slices were incubated at 35°C for a recovery period of 1 hr. After recovery, slices were placed in a submerged recording chamber (31°C; Warner Instruments) and continuously perfused (2 mL/min) with oxygenated ACSF. The glucose concentration used for recordings was 2.5 mM unless otherwise stated.

All drugs were applied to the perfusing system (bath application) to obtain the final concentrations indicated unless otherwise stated. Alpha-cyano-4-hydroxycinnamic acid (4-CIN), carbenoxolone disodium salt, sodium oxamate, sodium pyruvate, and tolbutamide were obtained from Sigma, sodium L-lactate from Alfa Aesar and tetrodotoxin citrate (TTX) from Tocris.

Patch-clamp recordings

Neurons and astrocytes located in the LHA were visually identified with a 16x objective and 2x magnification in an upright Nikon Eclipse FN1 microscope or with a 40x magnification in an upright Leica DM-LFSA microscope by using infrared differential interference contrast (IR-DIC). Whole-cell patch-clamp recordings were performed in current- and voltage-clamp modes by using a Multiclamp 700B amplifier (Molecular Devices). Data were filtered at 1 kHz and sampled at 5 kHz with Digidata 1322A interface

and Clampex 9.2 and 10.6 from pClamp software (Molecular Devices). Pipettes (from borosilicate capillaries; World Precision Instruments) had resistance of 6-8 MΩ when filled with an internal solution containing the following (in mM): 123 K-gluconate, 2 $MgCl_2$, 8 KCl, 0.2 EGTA, 4 Na_2-ATP, 0.3 Na-GTP, and 10 HEPES, pH 7.3 with KOH. Biocytin (2 mg/mL; Sigma) was also added to the internal solution for post hoc immunohistochemical phenotyping and evaluation of gap junctional coupling. For this latter, recordings were realized in current-clamp mode and limited to exactly 20 min. In some experiments, sodium L-lactate (2.5 or 5 mM; Alfa Aesar) was added to the internal solution. Loose patch-clamp recordings were performed in neurons in current-clamp mode and whole-cell configuration was achieved at the end of the experiment for electrophysiological and immunohistochemical characterization. All recordings were analyzed with Clampfit 9.2 and 10.6 from pClamp software (Molecular Devices). Instantaneous AP firing was calculated as the inverse of each AP interval. Junction potentials were determined to allow correction of membrane potential values. Orexin neurons exhibited tonic spontaneous firing (Figure 2A1), a H-current, a monophasic after hyperpolarizing potential and a low-threshold spike in response to 1 s negative and positive current pulses (from – 80 pA to 70 pA in 10 pA increments; Figures 4B and S2A). These electrophysiological membrane properties were different from those of melanin-concentratin hormone neurons residing in the same region (Eggermann et al., 2003; Parsons and Hirasawa, 2010). Electrical membrane properties of astrocytes was measured in voltage-clamp mode by applying a series of voltage pulses from – 100 mV to + 100 mV (300 ms, 10 mV increments) from a holding potential of – 80 mV. Input resistance (R_{in}) was determined by measuring the slope of the linear portion of the current-voltage (I-V) curve. Astrocytes in the LHA showed typical glial cell membrane properties (Steinhäuser, 1993; Sontheimer, 1994) characterized by the lack of AP firing in response to depolarizing current steps (Figure 4B), a linear current-voltage (I-V) relationship (Figures S4A1 and S4A2), a very negative RMP (–85.70 ± 1.05 mV; n = 17 cells from 5 animals; Figure S4C), and a low Rin (42.81 ± 6.70 MΩ; n = 17 cells from 5 animals; Figure S4D).

For glucose diffusion experiments, the internal solution contained the fluorescent glucose derivative 2-[N-(7-nitrobenz-2-oxa-1,3-diazol-4-yl)amino]-2-deoxyglucose (2-NBDG; 2 mg/ml; Invitrogen) and dextran tetramethylrhodamine (1 mg/ml; Molecular Probes). Recorded cells were loaded with these molecules during 20 min in current-clamp mode. Intercellular diffusion of fluorescent molecules was captured online with a digital camera exactly after 20 min and the number of coupled cells was analyzed offline with Fiji software.

For paired astrocyte-neuron whole-cell current-clamp recordings, one astrocyte was first recorded and filled with the gap junction-permeable tracer, Lucifer yellow CH dilithium salt (1 mg/ml; Sigma) through the patch pipette. Twenty min after basal astrocyte recording, one distant orexin neuron (intercellular distance of 50-75 μm) was recorded and filled with the membrane-impermeable dye, Alexa Fluor 594 hydrazide (40 μM; Invitrogen) through the patch pipette.

Cell phenotyping and dye-coupling analysis

Immediately after electrophysiological recordings, slices were fixed overnight with 4% paraformaldehyde in PBS solution (1x, pH 7.4) at 4°C and then rinsed several times with PBS solution and permeabilized and immunoblocked with 0.5% Triton X-100 and 5% NGS in PBS for 30 min at room temperature. For immunohistochemical phenotyping of recorded neurons filled with biocytin, slices were incubated with the rabbit anti-orexin-A primary antibody (1:1000; Millipore) in Triton/NGS/PBS for 3 days at 4°C. After several washes in 1x PBS solution, slices were incubated with the goat anti-rabbit Alexa Fluor 488 secondary antibody (1:500; Invitrogen) and streptavidin Alexa Fluor 546 (1:250; Invitrogen) in Triton/NGS/PBS overnight at 4°C. In some experiments, biocytin revelation was combined with double-immunolabeling for GFAP and NeuN to determine the phenotype of the coupled cells. To this end, slices were incubated with primary antibodies chicken anti-GFAP (1:1000; Abcam) and mouse anti-NeuN (1:1000; Millipore) in Triton/NGS/PBS for 3 days at 4°C and then treated with secondary antibodies goat anti-chicken Alexa Fluor 633 (1:500; Invitrogen) and goat anti-mouse Alexa Fluor 546 (1:500; Invitrogen) and streptavidin Alexa Fluor 488 (1:250; Invitrogen) in Triton/NGS/PBS overnight at 4°C. After several washes in 1x PBS solution, slices were mounted on slides and coverslipped with Vectashield antifade mounting medium. Fluorescent images were acquired with a confocal laser scanning microscope (Nikon A1). To determine the number of coupled cells, stack of optical sections at 3 μm intervals through the depth of the slice were obtained and images were analyzed by using Fiji software.

QUANTIFICATION AND STATISTICAL ANALYSIS

SigmaPlot 11 and 13 from Systat software were used to perform all statistical analysis. The difference between several groups was analyzed by one-way ANOVA. Two-way ANOVA was used when more than two comparisons (with time and genotype) were made. Repeated-measures ANOVAs were used when multiple measurements were made over time in the same groups. ANOVA was followed by the Student–Newman–Keuls or the nonparametric Dunn's post hoc multiple comparisons tests. Comparisons between two groups were conducted with the paired or unpaired Student's t test or the nonparametric Mann–Whitney test as appropriate. The level of significance was set at $p < 0.05$. Data are presented as mean ± SEM.